Title

ELECTRONIC PROPERTIES OF COMPLEX CRYSTALLINE AND AMORPHOUS PHASES OF Ge AND Si. II. BAND STRUCTURE AND OPTICAL PROPERTIES

Authors

Joannopoulos, J.D.
Cohen, Marvin L.

Publication Date

1973-05-01

Submitted to
Physical Review

LBL-1826
Preprint

ELECTRONIC PROPERTIES OF COMPLEX CRYSTALLINE AND AMORPHOUS PHASES OF Ge AND Si. II. BAND STRUCTURE AND OPTICAL PROPERTIES

J. D. Joannopoulos and Marvin L. Cohen

May 1973

Prepared for the U. S. Atomic Energy Commission
under Contract W-7405-ENG-48

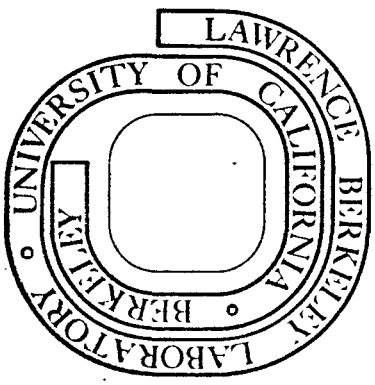

DISCLAIMER

Electronic Properties of Complex Crystalline and Amorphous Phases of Ge and Si. II. Band Structure and Optical Properties.*

J. D. Joannopoulos and Marvin L. Cohen

Department of Physics, University of California, Berkeley, Ca. 94720

and

Inorganic Materials Research Division, Lawrence Berkeley Laboratory

Berkeley, Ca. 94720

Abstract

We present calculations of the band structures and imaginary part of the dielectric function ϵ_2 as a function of energy for Ge and Si in the diamond, wurtzite, Si III (BC-8) and Ge III (ST-12) structures using the Empirical Pseudopotential Method. In particular we have obtained the symmetries of wavefunctions along important symmetry directions and identified the major contributions to the optical structure. A further study is made into the optical properties of amorphous Ge and Si using our short-range disorder model. We find that, unlike long range disorder models, short range disorder can explain both the amorphous density of states and the amorphous ϵ_2. In particular we find that the ϵ_2 spectrum has the same form as an averaged matrix element as a function of frequency.

I. INTRODUCTION

In a previous[1] paper (hereafter referred to as I) we calculated the band structure and density of states of Ge and Si in the

diamond (FC-2), wurtzite (2H-4), Si III (BC-8), and Ge III (ST-12) structures using the Empirical Pseudopotential Method (EPM). The trends observed with the increasing complexity of the structures indicated that short-range disorder (deviations in bond angles and bond lengths--which also provide for the presence of odd numbered rings--while all bonds are satisfied) was able to account well for the density of states of amorphous Ge and Si. This suggested that various distinctive features in the amorphous density of states[2] could be attributed to certain structural aspects of the amorphous phase. For example, deviations in the bond angles could be related to the shifting of states at the top of the valence band to higher energies for the amorphous case and the presence of odd-numbered rings of bonds in ST-12 led us to an argument that suggests that five and seven fold rings of bonds are responsible for the introduction of states between the two s-like peaks in the amorphous density of states.

In this paper we are concerned with the spectra of the imaginary part of the dielectric function ϵ_2 for the aforementioned structures. From a band structure point of view we present a detailed analysis of the structure in ϵ_2 for Ge and Si in the 2H-4, BC-8, and ST-12 cases along with their band structures containing the symmetries of wavefunctions along important directions. This is of interest since the BC-8 and ST-12 structures may have a variety of applications, e.g. exciton droplets and when doped, superconductivity. From the point of view of understanding the amorphous phase the trends observed in ϵ_2 as the structures become more and more complex may give some insight into the amount of disorder

necessary to produce the distinctive features of the amorphous ϵ_2. We shall show that our short range disorder model is the only theoretical model until now that can account for both the amorphous density of states and the amorphous ϵ_2[3,4]. In particular we shall show that when one measures the amorphous ϵ_2 spectrum one is essentially just measuring an averaged energy dependent matrix element.

The method of our calculations, the parameters used, and a description of the crystals studied were given in I and will not be repeated here.

In Section II we give a brief group theoretical analysis of the crystals and a description of the notation used in labelling the band structures. In Section III we give an analysis of the ϵ_2 spectra. In Section IV we present and discuss results which are of interest to the amorphous data. Finally, in Section V we make some concluding remarks. The reader interested only in the amorphous phase may proceed to sections IV and V with no loss in continuity.

II. SYMMETRY CONSIDERATIONS

We find that the 2H-4 structure has a symmetry classification of D_{6h}^4 and is therefore associated with a non-symmorphic space group. The BC-8 and ST-12 structures[5] have symmetry classifications T_h^7 and D_4^4 respectively and are thus also associated with space groups which are non symmorphic. The Brillouin zones (BZ) for these structures are shown in Fig. 1 with the notation used by Leurhmann.[6] In order to label the symmetries of our wavefunctions, shown in Figs. 2, 4, 6, 8, 9 and 11, we have used the notation for point group elements and the character tables found in Zak.[7] In our case, of course, these point operations must be followed by the appropriate translations. However, several remarks must be made relating to the additional symmetry, in some cases, demanded by time reversal

invariance, and to the symmetry notation for points located in the interior of the zone.

In the 2H-4 (D_{6h}^4) structure time reversal invariance adds additional symmetry to R. Thus R_1 and R_2 in our notation are obtained from $R_1 + R_4$ and $R_2 + R_3$, respectively, using Zak's character table. In the case of M (D_{2h}) our notation is identified by replacing U^x and σ^x with U^1 and σ^1 in the character table for D_{2h} in Zak. For $\Sigma(C_{2v})$ we obtain our character table by replacing C_2, σ_v, and σ_v with U^1, σ , and σ^z respectively in the character table for C_{2v} in Zak. Similarly for $\Gamma(D_{6h})$ and $\Delta(C_{6v})$ our notation is identified by replacing σ_h, $3\sigma_v$ with σ^z, $\sigma^{(x)}$ and $3\sigma_v$, $3\sigma_d$ with $3\sigma^{(x)}$, $3\sigma^{(1)}$ respectively in the appropriate character tables found in Zak.

In the BC-8 (T_h^7) structure time reversal invariance adds additional symmetry to Λ, P, D, Γ, and H. Thus for $\Lambda(C_3)$, Λ_1 and Λ_2 in our notation is obtained from 1 and 2 + 3, respectively, using Zak's character table. Similarly for P, time reversal invariance requires P_1 remain P_1 and $P_2 + P_3$ becomes P_2. For $D(C_2)$, $D_1 + D_2$ becomes D_1 and for $\Gamma(T_h)$, 1 becomes Γ_1, 2 + 3 become Γ_2, 4 becomes Γ_3, 5 becomes Γ_4, 6 + 7 become Γ_5 and 8 becomes Γ_6. The character table for H is the same as for T_h; it can be treated the same way as Γ. In the case of $\Delta(C_{2v})$ our notation is identified by replacing C_2, σ_v, and σ_v with C_2^x, σ^y, and σ^z respectively in the character table for C_{2v} in Zak.

In the ST-12 (D_4^4) structure our notation regarding labelling of symmetry points and directions is that of Leuhrman, as mentioned before, and for this case it differs from Zak's notation. Aside from this, time reversal

invariance requires that U^y, M^z, S, R, T, M, and U^z have additional symmetry. Thus $Y_1 + Y_2$ using Zak's notation becomes U^y_1 using our notation. Similarly for M^z, we have M_1 becomes $M^z{}_1$, $M_2 + M_3$ become $M^z{}_2$, and $M_4 + M_5$ become $M^z{}_3$, and for S we have $S_1 + S_2$ become S. For R we have $A_1 + A_2$ become R_1, and for T, $T_1 + T_2$ become T_1. Finally for M we obtain M_1 from $R_1 + R_2$ and M_2 from $R_3 + R_4$ and for U^z we obtain $U^z{}_1$ from $W_1 + W_2$. In the case of $\Gamma(D_4)$, $\Delta(C_2)$, $\Sigma(C_2)$, and $\Delta^z(C_4)$, which are internal symmetry points, our notation is identified using the character tables for D_4, C_2, C_2, and C_4 respectively found in Zak.

III. Band Structures and Optical Spectra

The band structures of Ge and Si in the 2H-4, BC-8, and ST-12 structures, shown in Figs. 2, 4, 6, 8, 9, and 11, were obtained from EPM calculations and the form factors used were given in I. In Figs. 3, 5, 7, 10 and 12 we show the ϵ_2 spectra calculated from these band structures using:

$$\epsilon_2(E) = \frac{1}{3} \cdot \frac{e^2\hbar^4}{\pi m^2 E^2} \sum_{c,v} \int_{BZ} \delta(E_c(\vec{k}) - E_v(\vec{k}) - E) \left| \langle \vec{k}, c | \vec{\nabla} | \vec{k}, v \rangle \right|^2 d^3\vec{k} \qquad (1)$$

where $|\vec{k}, v\rangle$ is a Bloch state in the valence band and the integral is over the entire BZ.

For the 2H-4 and ST-12 structures we can distinguish between the polarization of the electric vector and the c axis taken to be in the z-direction. In this case the factor of 1/3 in Eq. (1) is removed and we have parallel polarization if we use d/dz in the matrix element and perpendicular polarization if we use d/dx or d/dy. The integration was performed using

the Gilat-Raubenheimer scheme.[8] Tables I-VI summarize the major contributions to the various peaks in the ϵ_2 spectra for the six compounds. The first column identifies the energy of a particular peak and the second column contains the major contributions to this peak identified by interband transitions which are listed in order of decreasing strength. In particular, we list the bands which contribute more strongly once we are away from symmetry points and lines. The third column assigns the interband transitions to various regions of the BZ. Finally, in columns four and five we list the symmetries of the critical points and their associated energies respectively. In some cases the symmetries were obtained from a preliminary analysis and warrant further investigation. These are designated in the Tables by a tilde.

The complexity of the BC-8 and the ST-12 structures introduces the possibility that we may have critical points which are also inflection points along certain directions. Although it is rather difficult to determine this, it is conceivable that some of the critical points whose symtries are uncertain may be of this type.

For completeness we present an analysis for all six compounds and although experimental optical data are not available at the present, the contributions and identification of strong interband transitions to the optical properties will not vary appreciably with small changes in the form factors.

A. Ge 2H-4

The threshold in $\epsilon_2^{\perp}$ (Figs. 2 and 3) at 1.46 eV is caused by $\Gamma_5 - \Gamma_8$ transitions and the threshold in $\epsilon_2^{\parallel}$ at 1.77 eV is caused by $\Gamma_1 - \Gamma_8$ transitions. The rise in $\epsilon_2^{\perp}$ around 2.25 eV is caused by $\Gamma_6 - \Gamma_{10}$ transitions which are associated with an M_0 critical point (cp) and a region along $\Delta(\Delta_6 - \Delta_3)$ with small energy derivatives and large matrix elements. The shoulder at 2.25 eV is caused by an M_1 cp and associated transitions $A_3 - A_1$ at 2.26 eV. The small shoulder near 2.50 eV in $\epsilon_2^{\parallel}$ seems to be caused by an M_0 cp

near the center of the ΓALM face from bands 7-9. However, the shoulder near 2.50 eV in $\epsilon_2^{\perp}$ is caused by $\Delta_5 - \Delta_1$ transitions and an M_1 cp approximately 3/5 of the way from Γ to A. The small peak at 2.68 eV in $\epsilon_2^{\perp}$ is caused by $U_4 - U_2$ transitions and what seems like an M_1 cp at about 7/10 of the way from M to L. Although regions off symmetry directions around this critical point also contribute to $\epsilon_2^{\parallel}$ near 2.68 eV, this effect is overshadowed by $U_2 - U_2$ transitions and an M_1 cp near (0.5,0,0.4) at about 2.78 eV. These transitions are responsible for the peak observed around 2.75 eV in $\epsilon_2^{\parallel}$. The shoulder near 3.15 eV in $\epsilon_2^{\parallel}$ is caused by 7-10 transitions from a region near the T symmetry direction from an M_0 critical point at about (0.08,0.08,0.2) with energy 3.03 eV. In addition 7-9 transitions contribute to this shoulder from a probable M_2 cp at 3.14 eV and near (0.11,0.11,0.2). The shoulder in $\epsilon_2^{\perp}$ at 3.35 eV is caused by transitions from bands 6-9 in a large region mainly in the ΓALM plane around an M_1 cp approximately at (0.2,0,0.25). A similar shoulder in $\epsilon_2^{\parallel}$ at 3.57 eV is caused by a region with large matrix elements around what appears to be an M_1 cp near (0.2,0.2,0.35) at about 3.57 eV. The strongest peak in $\epsilon_2^{\perp}$ occurs at 3.60 eV and is caused mainly by 6-9 transitions in a large region with strong matrix elements around $M_7 - M_1$ particularly along $U_3 - U_1$ and $\Sigma_4 - \Sigma_1$. However, additional strength is obtained by 8-10 transitions in a region around $R_2 - R_1$ about 1/2 of the way from A to L and from an M_2 cp near (0.2,0,0.4) at 3.80 eV. The matrix elements are large for $\hbar\omega < 3.80$ eV and very small for $\hbar\omega > 3.80$ eV. The largest peak in $\epsilon_2^{\parallel}$ occurs at 3.72 eV caused mainly by an M_1 cp near H at the same energy. The peak in $\epsilon_2^{\perp}$

at 4.52 eV is caused by small contributions from three different interband transitions. The main contribution is from 8-11 transitions in a region (U_4 U_2) around $L_2 - L_1$, tentatively designated an M_0 cp at 4.40 eV. A slightly weaker contribution is from bands 8-9 caused by a region around the T symmetry direction with what seems like an M_0 cp near (0.23,0.23,0) at 4.45 eV. The final contribution to the peak at 4.52 eV for $\epsilon_2^{\perp}$ is probably caused by an M_1 cp near the center of the ΓALM face at 4.53 eV. This critical point provides the strongest contribution to the peak at 4.52 eV for $\epsilon_2^{\parallel}$ because of large matrix elements. The other main contribution to this peak is caused by 8-9 transitions with an M_2 cp at K and a region along T'. The shoulder around 4.70 eV in $\epsilon_2^{\perp}$ is mainly caused by 7-9 transitions with a probable M_2 cp at K and a small region extending along T'. Additional contributions to this shoulder are from 8-9 transitions in a small region around (0.4,0.15,0.15) with an M_3 cp at 4.72. The final contribution to this shoulder is from a region around A particularly along S with a probable an M_2 cp near (0.03,0.03,0.45) at 4.71 eV. The shoulder in $\epsilon_2^{\parallel}$ around 4.70 eV is caused by an M_0 cp near M about 0.1 of the way along T' and from 7-9 transitions in a region near K along P with a probable M_3 cp at about 4.9 eV near (0.33,0.33,0.15). The last discernible peak in $\epsilon_2^{\perp}$ occurs at 5.23 eV and is caused mainly by $\Gamma_5 - \Gamma_{12}$ transitions which are associated with an M_2 cp at 5.23 eV. Additional contributions to this peak are from 8-11 transitions ina small region around (0.08,0.08,0.35) which has an M_3 cp at 5.30 eV. The last discernible shoulder in $\epsilon_2^{\parallel}$ around 5.29 eV is caused by $M_5 - M_4$ and $\Sigma_3 - \Sigma_4$ transitions at 5.33 eV and 5.31 respectively. We

have not determined the symmetry of these critical points. Other contributions to this shoulder are from 8-11 transitions in a small region around (0.3,0.1,0.15) at 5.29 eV.

B. Si 2H-4

The threshold in $\epsilon_2^{\perp}$ (Figs. 4 and 5) at 2.60 eV is caused by $\Sigma_1 - \Sigma_1$ transitions and a probable M_0 cp near (0.3,0,0) while the region around this cp off symmetry directions contributes to the threshold in $\epsilon_2^{\parallel}$ at nearly the same energy. The first shoulder in $\epsilon_2^{\parallel}$ at 3.10 eV is caused by an M_0 cp near the center of the ΓALM face from bands 7-9. The next shoulder in $\epsilon_2^{\parallel}$ occurs around 3.35 eV and is caused by $U_2 - U_2$ transitions with an M_1 cp near (0.5,0,0.35) at about 3.34 eV. The rise in $\epsilon_2^{\perp}$ around 3.35 eV is caused by $\Gamma_6 - \Gamma_{10}$ transitions which are associated with an M_0 cp and a region along $\Delta(\Delta_6 - \Delta_3)$. The shoulder at 3.35 eV is caused by an M_1 cp and associated transitions $A_3 - A_1$. The next shoulder in $\epsilon_2^{\perp}$ at 3.60 eV is a result of $\Delta_5 - \Delta_1$ transitions and an M_1 cp approximately 1/2 of the way from Γ to A. The largest peak in $\epsilon_2^{\perp}$ at 4.10 eV is caused mainly by 6-9 transitions in a large region with strong matrix elements around $M_7 - M_1$ particularly along $U_3 - U_1$ and $\Sigma_4 - \Sigma_1$. To a much lesser extent additional strength to this peak is obtained from a region around $R_2 - R_1$, specifically 1/2 of the way from A to L. Here we find an M_2 cp near (0.15,0,0.5) at about 4.13 eV. The first large peak in $\epsilon_2^{\parallel}$ occurs around 4.25 eV and is caused by a region with large matrix elements around what appears to be an M_1 cp near (0.2,0.2,0.35) at about 4.21 eV. In addition a region near H along S' which also has large matrix elements contributes around 4.26 eV.

The shoulder at $\epsilon_2^{\perp}$ near 4.38 eV is a result of an M_2 cp around (0.2,0,0.4) at 4.38 eV and transitions in a region around $R_2 - R_1$ near (0.2,0,0.5). The second large peak in $\epsilon_2^{\parallel}$ occurs around 4.68 eV and is the result of several contributions. First we have 8-10 transitions in a region near M about 0.2 of the way along T' where we have a probable M_2 cp at 4.64 eV. Next there are 8-9 transitions in a small region around (0.3,0.1,0) with an M_1 cp at 4.68 eV and 7-11 transitions with an M_0 cp at 4.61 near (0.4,0, 0.35). Finally, we have contributions from the shoulder of a non-discernible peak around 4.75 eV caused by 7-9 transitions along T with what is probably an M_2 cp at 4.74. The peak in $\epsilon_2^{\perp}$ at 4.69 eV is caused mainly by 8-9 transitions along the T symmetry direction with an M_0 cp at 4.57 eV and to a lesser extent from $\Delta_6 - \Delta_5$ transitions with what seems like an M_1 cp at 4.69 eV near (0,0,0.3). The peak in $\epsilon_2^{\perp}$ at 4.89 eV is a result of what appears to be an M_2 cp at K around 4.87 eV and a probable M_2 cp near (0.3,0.25,0.25) around 4.89 eV. The shoulder in $\epsilon_2^{\parallel}$ at 4.91 eV is caused by a probable M_2 cp for 7-10 and 8-10 transitions at 4.91 eV and 4.93 eV near (0.2,0.08,0) and (0.2,0.1,0) respectively. The shoulder in $\epsilon_2^{\perp}$ at 4.96 eV is caused mainly by 8-11 transitions slightly off the Σ direction at a probable M_2 cp near (0.35,0.05,0.05) at 4.96 eV, while the shoulder at 5.50 eV is a result of $\Gamma_5 - \Gamma_{12}$ transitions with an associated M_1 cp at 5.47. Finally the shoulder around 5.55 eV in $\epsilon_2^{\parallel}$ is caused by $M_5 - M_4$ and $\Sigma_3 - \Sigma_4$ transitions at 5.61 and 5.54 eV respectively.

C. Ge BC-8

The first peak in ϵ_2 (Figs. 6 and 7) at 2.03 eV is caused by $\Sigma_1 - \Sigma_2$

transitions with an M_1 cp about 4/5 of the way from Γ to N. The shoulder at 2.46 is caused by a small region around $\Sigma_2 - \Sigma_2$ with a probable cp near (0.4,0.4,0) at 2.46 eV whose symmetry we have not determined. Additional contributions to this shoulder are from $\Delta_4 - \Delta_4$ transitions and an M_0 cp about 1/2 the way along Δ at 2.41 eV. The main contribution to the peak at 2.70 eV is from 13 - 17 transitions in a small region around an M_0 cp near (0.2,0.8,0.15) at 2.67 eV. A smaller contribution is from $G_2 - G_1$ transitions with what appears to be on M_0 cp near (0.15,0.85,0) at 2.65 eV. The large peak at 3.21 eV is a result of many contributions. First/16 - 19 transitions in a region of large matrix elements around an M_0 cp near (0.25,0.35,0.25) at 3.19 eV. Next/$G_1 - G_2$ transitions with an M_2 cp near (0.4,0.6,0) at 3.24 eV and a region of large matrix elements around (0.3, 0.4,0.15) at about 3.23 eV. Thirdly/14 - 17 transitions in a region around (0.2,0.4,0.15) with what appears to be an M_2 cp at 3.21 eV. Finally,/13 - 18 transitions near (0.3,0.45,0) with an M_1 cp at 3.21 and $G_1 - G_1$ transitions with a probable cp at (0.22,0.78,0) whose symmetry we have not determined. The shoulder around 3.76 eV is also the result of several contributions. The first is from 15 - 19 transitions in a region near N with $G_2 - G_1$ transitions and an M_3 cp near (0.4,0.55,0) at 3.78 eV. Next/12 - 18 transitions near N with $G_2 - G_1$ transitions and an M_1 cp near (0.35,0.65,0) at 3.76 eV. Finally, we have contributions from a small region around Γ with $\Gamma_2 - \Gamma_6$ transitions and an M_3 cp at 3.74 eV. The shoulder at 3.98 eV is caused by 14 - 19 transitions in a large region around (0.25,0.65,0.15) at 4.0 eV. The last discernible peak occurs at 4.50 eV and is caused by 12 - 19

transitions in a region around (0.26,0.63,0.15) and 14 - 20 transitions in a large region around (0.1,0.5,0.1) both with strong matrix elements. In addition we have contributions from 16 - 21 transitions in a region around (0.15,0.2,0.1) with an M_2 cp near 4.48 eV and $\Delta_1 - \Delta_4$ transitions with an M_0 cp near (0.25,0,0) at 4.42 eV.

D. Si BC-8

The threshold in ϵ_2 (Figs. 7 and 8) at 0.43 eV is caused by $H_3 - H_4$ transitions. The small bump around 1.70 eV is a result of $\Delta_1 - \Delta_4$ transitions with an M_0 cp near (0.55,0,0) at 1.65 eV. The next small bump at 2.04 eV is caused by what appears to be an M_2 cp near (0.3,0.55,0). The shoulder at 2.60 eV is primarily caused by $\Sigma_1 - \Sigma_2$ transitions with an M_2 cp near (0.4,0.4,0) at 2.62 eV. Additional structure is obtained by 15-17 transitions in a region around an M_0 cp near (0.3,0.5,0) at 2.54 eV. The shoulder at 3.0 eV is caused by 13-17 transitions in a small region around an M_0 cp near (0.2,0.7,0.15) at 2.96 eV. The large peak at 3.45 eV is the result of many contributions. The first is from 13-17 transitions in a region of very large matrix elements around (0.1,0.5,0.1) at about 3.46 eV. Next we have 14 - 17 transitions in a region around what appears to be an M_2 cp near (0.2,0.4,0.15) at 3.45 eV with strong matrix elements. Also, there are 16-19 transitions in a small region with very large matrix elements and an M_1 cp near (0.3,0.4,0.2) at 3.43 eV. Finally there is a region around $\Gamma_1 - \Gamma_6$ transitions with an associated M_0 cp at 3.38 eV.

The shoulder at 3.7 eV is caused by a small region around $G_1 - G_2$ transitions with an M_2 cp at 3.7 eV near (0.45,0.55,0) and by a small region around

$D_1 - D_1$ transitions with large matrix elements and an M_1 cp at 3.68 eV around (0.5,0.5,0.15). The shoulder at 4.05 eV is the result of several types of transitions. First we have 16 - 21 transitions in a small region around (0.2,0.6,0.15) with large matrix elements and $\Delta_1 - \Delta_2$ transitions with an M_2 cp near (0,5,0,0) at 4.04 eV. Next we have 15-21 transitions in a small region around (0.2,0.6,0.1) with an associated M_0 cp at 4.02 eV and $G_1 - G_1$ (13 - 18) transitions with a probable cp near (0.2,0.8,0) whose symmetry we have not yet determined. Finally we have 14 - 19 transitions in a region around what appears to be an M_1 cp near (0.25,0.65,0.1) at 4.07 eV. The large peak at 4.20 eV is mainly caused by 16 - 22 transitions in a region of very large matrix elements around what appears to be an M_2 cp near (0.2, 0.5,0) at 4.20 eV. In addition we have contributions from 12 - 18 and 15 - 22 transitions in a small region around an M_2 cp near (0.15,0.7,0.15) at 4.22 eV and an M_0 cp near (0.15,0.7,0) at 4.14 eV respectively. Finally the shoulder at 5.05 eV can be attributed to 14 - 21 transitions in a small region around an M_2 cp near (0.2,0.6,0.1) at 5.05 eV and $D_1 - D_1$ transitions with a probable cp near (0.5,0.5,0.1) at 5.0 eV whose symmetry we have not determined.

E. Ge ST-12

In this section and the section on Si ST-12 we shall treat the perpendicular component of $\epsilon_2^{\perp}$ first and discuss the parallel component in the last paragraph.

The threshold in $\epsilon_2^{\perp}$ (Figs. 9 and 10) occurs at 1.46 eV and is caused by $\Sigma_1 - \Sigma_1$ transitions. The shoulder at 2.10 eV is caused by equal contributions from 24 - 25 and 23 - 25 transitions in small regions (tubular along

the z direction) around an M_0 cp near (0.4,0.1,0.3) at 2.08 eV and an M_1 cp near (0.4,0,0.3) at 2.18 eV respectively. The shoulder around 2.55 eV is caused mainly by 24 - 26 transitions in a region around an M_1 cp near (0.5,0.1,0.3) at 2.48 eV along with much weaker contributions from $T_1 - T_1$ (0.5,0.5,0.4) and $U_1^z - U_1^z$ (0.5,0,0.3) transitions at 2.52 eV and 2.50 eV respectively whose critical point symmetries have not been determined. Next we have 23 - 26 transitions in a region of relatively large matrix elements around (0.4,0.15,0.25) contributing at 2.62 eV. Other contributions to this shoulder are from 22 - 25 and 21 - 25 transitions, with a probable M_2 cp near (0.4,0,0.25) at 2.62 eV and an M_1 cp near (0.4,0.15,0.25) at 2.60 eV respectively, along with transitions at M in a much weaker sense at 2.60 eV. Finally, we have 24 - 25 transitions with an M_0 cp near (0.1,0.1,0.4) at 2.54 eV.

The peak around 2.80 eV is the result of several types of transitions whose contributions are all of comparable weight. First we have 23, 24 - 26 transitions in a region (mostly along z direction) around $S_1 - S_1$ with an M_2 cp near (0.4,0.4,0.5) at 2.87 eV. Next there are 21 - 25 transitions in a region around an M_1 cp near (0.4,0.15,0.25) at 2.60 eV which contributes to 2.75 eV because of matrix elements and in a weaker sense $\Delta_1 - \Delta_1$ (0.4,0,0) transitions with a cp of undetermined symmetry at 2.80 eV. Next we have 24 - 25 transitions near the U^x symmetry direction with an M_1 cp near (0.2,0,0.4) at 2.70 eV. Finally, we have 24 - 27 transitions in a small region (tubular along z-direction) around an M_1 cp near (0.5,0.1,0.3) at 2.76 eV along with some weaker $\Gamma_3 - \Gamma_5$ transitions with an M_0 cp at 2.75 eV.

The shoulder around 3.0 eV is caused mainly by 20 - 25 transitions in a region (tubular along z-direction) around an M_0 cp near (0.4, 0.15, 0.25) at 2.93 eV and 22 - 25 transitions in a region around Z_2 - Z_2 with an associated M_0 cp at 2.98 eV along with much weaker T_1 - T_1 (0.5, 0.5, 0.3) transitions at 3.0 eV. Additional contributions to this shoulder are from 24 - 27 transitions in a small region near R along T^z with an M_1 cp near (0.5, 0.5, 0.45) at 3.11 eV and 19 - 25 transitions in a region of relatively large matrix elements around (0.35, 0.18, 0) at 2.97 eV along with weaker M_2^z - M_1^z transitions with what appears to be an M_2 cp at 3.0 eV. Finally, we have 22 - 27 transitions with an M_0 cp near (0.5, 0.15, 0.3) at 3.04 eV.

The next shoulder around 3.20 eV is caused mainly by Z_1 - Z_1 transitions with an associated M_0 cp at 3.18 eV along with much weaker transitions Z_1^x - Z_1^x with an M_3 cp at 3.20 eV. Other contributions to this peak are from 21 - 25 transitions in a small region around U^x with an M_2 cp near (0.2, 0, 0.5) at 3.21 eV and 23 - 28 transitions in a region (tubular along z-direction) near R mostly along T^z with a probable M_1 cp at 3.20 eV. Finally, we also have contributions from 19 - 25 transitions with an M_2 cp near (0.5, 0.15, 0.3) at 3.21 eV along with weaker Δ_1 - Δ_1 transitions near (0.38, 0, 0) at 3.20 eV. The peak at 3.50 eV is caused mainly by 19 - 25, 26 transitions and a region (along z-direction) around R_1 - R_1 with an M_0 cp at 3.46 eV and 18 - 25 transitions in a small region around T_1 - T_1 near (0.5, 0.22, 0.5) with a probable M_0 cp at 3.49 eV. Additional contributions are from S_1 - S_1 (20 - 25) transitions with an M_0 cp near (0.06, 0.06, 0.5) at 3.45 eV and what appears to be an M_1 cp near (0.45, 0.45, 0.5) also at 3.45 eV. Other contri-

butions are from 17 - 25 transitions in a small region along T^z near (0.5, 0.5, 0.3) with a probable M_1 cp at 3.53 eV and 24 - 27 transitions with a probable M_2 cp near (0, 0.1, 0.25) at 3.47 eV and to a lesser extent $T_1 - T_1$ transitions near (0.5, 0.3, 0.5) at about 3.50 eV. Finally, we have $T_1 - T_1$ (20 - 26) transitions with an M_2 cp at 3.47 eV and 22 - 27 transitions with an M_2 cp near 3.54 eV and to a lesser extent $\Delta_1 - \Delta_1$ transitions near (0.45, 0, 0) contributing at 3.50 eV.

The shoulder at 3.65 eV is caused by 17 - 25 transitions in a region (tubular along z-direction) around an M_2 cp at 3.67 eV near (0.5, 0.25, 0.3) and in a weaker sense by $Z_1 - Z_2$ transitions with an M_0 cp at 3.65 eV. Other contributions to this shoulder are from 23 - 27 transitions in a relatively large region around (0.1, 0, 0.25) which contributes around 3.65 eV, 24 - 29 transitions in a region around U^x with an M_0 cp near (0.22, 0, 0.5) at 3.60 eV, and 24 - 30 transitions at R with an M_1 cp at 3.60 eV. The peak at 4.20 eV is caused by 24 - 30 transitions in a region (mostly in z-direction) near U^x around (0.3, 0, 0.4) which contributes at about 4.18 eV along with weaker transitions in a region around M at 4.20 eV. In addition we have 21 - 27 transitions with an M_2 cp near (0.15, 0.15, 0.2) at 4.22 eV and 23 - 28 transitions in a region around $\Delta_2 - \Delta_1$ with most of the contributions near (0.1, 0, 0.05) at 4.20 eV. Other transitions contributing to this peak are 21 - 28 transitions in a small region near U^x around (0.15, 0, 0.4) at 4.20 eV and 20 - 25 transitions around $\Sigma_2 - \Sigma_1$ with an M_1 cp near (0.07, 0.07, 0) at 4.21 eV. Finally, we also have some weak structure from $S_1 - S_1$ (23 - 32) transitions with a cp of undetermined symmetry near (0.22, 0.22, 0.5) at

4.20 eV.

The last peak that we shall consider in $\epsilon_2^{\perp}$ occurs at 4.50 eV and is the result of many different contributions. First we have 23 - 31 transitions in a region around U_1^z - U_1^z with a probable M_3 cp near (0.5,0,0.2) at 4.57 eV and Σ_2 - Σ_1 (21 - 23) transitions with a cp of undetermined symmetry near (0.4,0.4,0) at 4.48 eV. Next we have 22- 30 transitions in a small region near U^y with an M_1 cp around (0.45,0.1,0.05) at 4.36 eV and an M_1 cp near (0.3,0.15,0.4) at 4.52 eV. In addition we have 20 - 26 transitions with an M_3 cp near (0.15,0,0.1) at 4.54 eV and 20 - 28 transitions with an M_0 cp near (0.15,0.15,0.25) at 4.47 eV. Finally for completeness we also list in Table III a set of much weaker transitions along symmetry directions at critical points of undetermined symmetry, starting with M_3^z - M_1^z transitions and ending with U_1^y - U_1^y transitions. Taken as a whole they are of comparable weight to the others discussed above.

The threshold in $\epsilon_2^{\parallel}$ occurs around 1.60 eV with minute matrix elements from Σ_2 - Σ_1 transitions at 1.46 eV and very small matrix elements near 1.6 and appreciable contributions only from Δ_2 - Δ_1 transitions with a probable M_1 cp near (0.4,0,0) at 1.7 eV. The shoulder around 2.15 eV is caused mainly by Σ_2 - Σ_1 transitions with an M_0 cp near (0.37,0.37,0) at 2.07 eV. In addition we have contributions from 24 - 25 and 23 - 25 transitions in small regions around what appears to be an M_0 cp near (0.4,0.1,0.3) at 2.08 eV and an M_1 cp near (0.4,0,0.3) at 2.18 respectively. The shoulder around 2.65 eV is caused mainly by 21 - 15 transitions in a region around an M_1 cp near (0.4,0.15,0.25) and 2.60 eV and a region (particularly along U^y) around

$Z_1^x - Z_1^x$ with a probable M_2 cp at 2.65 eV and $U_1^y - U_1^y$ transitions contributing at 2.63 eV. Additional contributions are from 22 - 26 transitions with an M_1 cp near (0.5,0.2,0.25) at 2.74 eV and 22-25 transitions in a region around $M_3^z - M_1^z$ with a probable M_2 cp at 2.70 eV. Finally, to a much lesser extent, we have contributions from $\Gamma_3 - \Gamma_4$ transitions with an M_0 cp at 2.64 eV.

The peak at 3.20 eV is a result of several interband contributions of approximately the same weight. First we have 24 - 27 transitions in a region around $Z_1 - Z_1$ with an M_0 cp at 3.18 eV along with weaker $Z_1^x - Z_1^x$ transitions with an M_3 cp at 3.20 eV and $\Delta_2 - \Delta_1$ transitions with a probable M_2 cp near (0.45,0,0) at 3.18 eV. Next we have 21 - 25 transitions in a small region (mostly along z-direction) around U^x with an M_2 cp near (0.2,0,0.5) at 3.21 eV and a region of large matrix elements near (0.2,0.2,0.3) contributing to 3.20 eV. In addition we have 24 - 26 transitions in a region around $S_1 - S_1$ with an M_3 cp near (0.26,0.26,0.5) at 3.26 eV and in a weaker sense $R_1 - R_1$ (23 - 28) transitions at 3.20 eV and $\Sigma_2 - \Sigma_1$ (24 - 28) transitions with a probable M_1 cp near (0.25,0.25,0) at 3.20 eV. The next peak at 3.50 eV is a result, in part, of 20 - 25 transitions in a region around $Z_2 - Z_2$ with a cp of undetermined symmetry at 3.48 eV and $S_1 - S_1$ transitions with an M_0 cp near (0.06,0.06,0.5) at 3.45 eV. In addition there are contributions from 22 - 27 transitions in a small region around an M_2 cp near (0.3,0.1, 0.3) at 3.54 eV, $\Gamma_5 - \Gamma_5$ transitions with an associated M_0 cp at 3.44 eV and 20 - 26 transitions in a region (tubular along z-direction) of relatively large matrix elements around (0.3,0.1,0.3) at 3.53 eV. Finally, there are weaker contributions from $\Sigma_2 - \Sigma_1$ (24 - 29) and $\Delta_1 - \Delta_2$ (24 - 26) transitions

with critical points of undetermined symmetry near (0.35,0.35,0) at 3.45 eV and near (0.3,0,0) at 3.48 eV respectively.

The shoulder at 3.70 eV is caused by 24 - 28 transitions in a small region around $\Delta_1 - \Delta_2$ with a cp of undetermined symmetry near (0.26,0,0) at 3.70eV and S_1-S_1 transitions with a probable M_2 cp near (0.2,0,0) also at 3.70 eV. Other contributions to this shoulder are from 21 - 27 transitions around $Z_1^X - Z_1^X$ with an M_1 cp at 3.69 eV and $U_1^Z - U_1^Z$ transitions with a cp of undetermined symmetry near (0.5,0,0.2) at 3.71 eV. The peak at 3.90 eV is caused in part by 19 - 25 transitions in a small region (mostly in z-direction) around an M_3 cp near (0.2,0.15,0.3) at 3.92 eV and 24 - 29 transitions around $\Delta_2^Z - \Delta_2^Z$ with an M_2 cp near (0,0,0.18) at 3.94 eV. Additional contributions are from 23 - 29 transitions around $\Delta_1 - \Delta_2$ with what appears to be an M_2 cp at 3.9 eV, $S_1 - S_1$ transitions with a cp of undetermined symmetry at 3.9 eV, and $\Delta_2 - \Delta_1$ (21 - 26) transitions with a probable M_1 cp near (0.15,0,0) at 3.88 eV. The peak at 4.20 eV is caused in part by 24 - 29 transitions in a region of very large matrix elements around $\Gamma_3 - \Gamma_4$ with an M_3 cp at 4.22 eV and 20 - 25 transitions in a region around $\Gamma_3 - \Gamma_4$ with an M_0 cp at 4.16 eV along with an M_1 cp near (0.07,0.07,0) at 4.21 eV from $\Sigma_2 - \Sigma_1$ transitions. Other contributions to this peak are from 21 - 28 transitions in a region around $\Gamma_2 - \Gamma_1$ with an M_0 cp at 4.22 eV including in particular $\Delta_1^Z - \Delta_1^Z$ transitions at 4.23 eV, transitions in a small region near U^X around (0.15,0,0.4) at 4.20 eV, and to a lesser extent $S_1 - S_1$ transitions with a cp of undetermined symmetry at 4.20 eV. Still other contributions are from 22 - 29 transitions with an M_0 cp near (0.15,0.15,0.2) at 4.21 eV

and weaker $Z_1^x - Z_1^x$ transitions with an M_2 cp at 4.24 eV. Finally, we have 24 - 30 transitions with an M_1 cp near (0.1,0.1,0.3) at 4.26 eV and 22 - 30 transitions in a region around (0.3,0.25,0.25) contributing at 4.21 eV.

The last peak that we shall consider in $\epsilon_2^{\parallel}$ occurs at 4.40 eV and is the result of many different contributions. First we have 20 - 26 transitions in a region (tubular along z-direction) around an M_2 cp near (0.17,0.17, 0.1) at 4.42 eV and 18 - 27 transitions in a region around $Z_1 - Z_1$ with an M_0 cp at 4.36 eV. Next we have 23 - 28 ($\Sigma_1 - \Sigma_2$) transitions and 22 - 27 ($\Sigma_1 - \Sigma_2$) transitions with critical points of undetermined symmetry near (0.14, 0.14,0) at 4.40 eV and 4.37 eV respectively along with $\Delta_1 - \Delta_2$ transitions with a cp near (0.25,0,0) at 4.40 eV. Other contributions are from 23 - 24 transitions around $M_2^z - M_1^z$, with a probable M_2 cp at 4.40 eV and $\Sigma_1 - \Sigma_2$ transitions with a cp of undetermined symmetry near (0.35,0.35,0) at 4.40 eV. In addition we have weaker contributions from 16 - 26 transitions in a small region around $Z_2 - Z_2$, particularly along $\Delta_2^z - \Delta_3^z$ at 4.40 eV, with a probable M_1 cp at 4.37 eV. Finally we have 23 - 30 transitions with an M_3 cp near (0.35,0.15,0.3) at 4.42 eV, $\Delta_1 - \Delta_2$ transitions with a cp of undetermined symmetry near (0.37,0,0) at 4.40 eV, and 22-31 transitions around $U_1^y - U_1^y$ with a cp near (0.5,0.3,0) at 4.40 eV.

F. Si ST-12

The threshold in $\epsilon_2^{\perp}$ (Figs. 11 and 12) occurs at 1.76 eV and is the result of 24 - 25 transitions around an M_0 cp near (0.4,0.2,0). The shoulder at 2.33 eV is caused by 23 - 25 transitions and 24 - 25 transitions in a region (tubular along z-direction) around an M_0 cp near (0.4,0,0.3) at 2.31 eV and around an M_1 cp near (0.4,0,0.45) at 2.33 eV respectively.

The shoulder at 2.50 eV is caused by 23 - 26 and mainly 24 - 26 transitions in a region around M with a probable M_1 cp at 2.50 eV. In particular, we have contributions from $T_1 - T_1$ transitions with an M_1 cp near (0.5,0.15,0.5) at 2.52 eV and $U_1^z - U_1^z$ transitions at 2.51 eV. Finally, we have weaker transitions from a region near Z^x along $U_1^y - U_1^y$ contributing to 2.45 eV.

The peak at 2.80 eV is a result in part of 23, 24- 26 transitions in a region around $S_1 - S_1$ (0.4,0.4,0.5) at 2.76 eV with particularly strong contributions off the symmetry axis with an M_1 cp near (0.4,0.4,0.4) at 2.80 eV. Other contributions are from 21 - 25 transitions with an M_0 cp near (0.45,0.15,0.3) at 2.73 eV, $\Delta_2 - \Delta_1$ transitions with a cp of undetermined symmetry near (0.45,0,0) at 2.80 eV, and $U_1^y - U_1^y$ transitions with an M_1 cp near (0.5,0.2,0) at 2.79 eV along with 22 - 26 transitions in a large region (along z-direction) around (0.5,0.3,0.15) contributing at 2.82 eV. Finally we have contributions from $Z_1 - Z_1$ (23 - 28) transitions with an M_0 cp at 2.78 eV and 22 - 25 transitions with an M_2 cp near (0.4,0,0.25) at 2.74 eV. The shoulder at 3.20 eV is caused mostly by 20 - 25 transitions in a region of relatively large matrix elements around $\Delta_1 - \Delta_1$, with an M_0 cp near (0.39,0,0) at 3.17 eV and a region around $\Sigma_1 - \Sigma_1$ with an M_2 cp near (0.37,0.37,0) at 3.21eV, along with 19-25 transitions in a region (along z-direction) around $\Sigma_1 - \Sigma_2$ with a probable M_1 cp near (0.4,0.4,0) at 3.18 eV. Additional contributions are from 22 - 25 transitions in a region around $Z_2 - Z_2$ with an M_0 cp at 3.18 eV and an M_1 cp near (0.2,0.2,0.25) at 3.16 eV and 20 - 26 transitions in a region around U^y with an M_1 cp near (0.5,0.35,0.05) at 3.17 eV and a cp of undetermined symmetry near (0.4,0.4,0) from $\Sigma_1 - \Sigma_1$ transitions at 3.20

eV. Other contributions are from 22 - 28 transitions, from a cp of undetermined symmetry around $U_1^y - U_1^y$ near (0.5,0.4,0) at 3.20 eV and $R_1 - R_1$ transitions at 3.20 eV, and 21 - 26 transitions in a region around T^z with an M_2 cp near (0.5,0.5,0.4) at 3.23 eV.

The largest peak in $\epsilon_2^\perp$ occurs at 3.38 eV and is the result of many types of transitions. First we have 20-25 transitions in a region near R along T^z with an M_1 cp near (0.5,0.5,0.45) at 3.39 eV and 19 - 25 transitions in a similar region around T^z with a probable M_3 cp near (0.48,0.48,0.4) at 3.45 eV, along with $\Sigma_2 - \Sigma_1$ transitions near (0.35,0.35,0) with a cp of undetermined symmetry at 3.35 eV. Next we have 22 - 26 transitions, with a large region (along z-direction) around an M_2 cp near (0.25,0.25,0.3) at 3.36 eV. Additional contributions are from 18 - 25 transitions, with an M_0 cp near (0.4,0.2,0) at 3.35 eV and $U_1^y - U_1^y$ transitions near (0.5,0.38,0) with a cp at 3.4 eV, and 24 - 27 transitions with an M_1 cp near (0.15,0,0.3) at 3.38 eV and $U_1^z - U_1^z$ transitions near (0.5,0,0.15) with a cp around 3.38 eV. Finally we have 22 - 28 transitions, with an M_0 cp at 3.37 eV from $Z_2 - Z_1$ transitions and an M_1 cp near (0.45,0.4,0.3) at 3.35 eV, and 23 - 27 transitions with contributions from various regions of the zone contributing at around 3.35 eV. The shoulder at 3.60 eV is caused in part by 20 - 25 transitions in a region near Z around U^x with an M_0 cp near (0.1,0,0.5) at 3.60 eV and 21 - 26 transitions with a probable M_1 cp near (0.3,0.2,0.25) also at 3.60 eV. Other contributions are from 22 - 27 transitions in a region around $\Sigma_2 - \Sigma_1$ with an M_0 cp near (0.3,0.3,0) at 3.50 eV, 21 - 29 transitions in a region around $R_1 - R_1$ with an M_0 cp at 3.59 eV and 23 - 27 transitions with an M_0 cp near (0.1,0.1,0.25) at 3.54 eV. Finally we have 23 - 28

transitions with an M_1 cp near (0.5,0.15,0.3) at 3.58 eV, 22 - 26 transitions in a region around $\Delta_2^z - \Delta_4^z$ with a cp of undetermined symmetry near (0,0, 0.3) at 3.60 eV and 22 - 28 transitions in a region around $\Sigma_2 - \Sigma_1$ with a cp near (0.32,0.32,0) at 3.60 eV.

The peak around 3.85 eV is the result of many types of transitions contributing approximately equally to $\epsilon_2^\perp$. First we have 24 - 29 transitions in a region around $Z_1^x - Z_1^x$ with an M_2 cp at 3.92 eV and 23 - 28 transitions in a region (tubular abng z-direction) around $\Gamma_5 - \Gamma_1$ with an M_0 cp at 3.71 eV along with $\Delta_4^z - \Delta_1^z$ transitions with an M_2 cp near (0,0,0.24) at 3.85 eV. Next we have 23 - 29 transitions in various regions of the zone with strongest contributions from a large tubular region in the z-direction around (0.35, 0.15,0.25) contributing at 3.85 eV and 17 - 25 transitions in a large region around $U_1^z - U_1^z$ (0.5,0,0.33) parallel to the T direction contributing at 3.85 eV. Other contributions are from 22 - 27 transitions, with a probable M_1 cp near (0.15,0.15,0.2) at 3.81 eV, 21 - 29 transitions, with contributions from a small region around $\Sigma_1 - \Sigma_2$ and an M_1 cp near (0.42,0.42,0) at 3.88 eV, and 20 - 26 transitions with what appears to be an M_1 cp near (0.15,0.1, 0.4) at 3.89 eV. Finally, we have 16 - 25 transitions in a region around $M_3^z - M_2^z$ with an M_1 cp at 3.86 eV and 23 - 20 transitions with a probable M_1 cp near (0.35,0.35,0.25) at 3.81 eV.

The last structure we shall consider in the $\epsilon_2^\perp$ spectrum occurs at 4.45 eV. This shoulder is caused in part by 20 - 26 transitions in a region (along z direction) around what appears to be an M_2 cp near (0.1,0,0.1) at 4.48 eV, $\Sigma_1 - \Sigma_1$ transitions with a cp of undetermined symmetry near

(0.12,0.12,0) at 4.44 eV and 23 - 25 transitions with a cp at M_2^z - M_3^z at 4.46 eV. Other contributions are from 15 - 27 transitions in a region around M_3^z - M_1^z with a probable M_1 cp at 4.45 eV and 15 - 26 transitions near M^z with a cp from Σ_2 - Σ_1 transitions near (0.44,0.44,0) at 4.42 eV along with U_1^z - U_1^z transitions with a cp near (0.5,0,0.34) at 4.45 eV. Next we have 14 - 26 transitions, with a cp at M_3^z - M_2^z at 4.41 eV and a cp from T_1 - T_1 transitions near (0.5,0.28,0.5) at 4.45 eV, and 21 - 27 transitions with a probable M_1 cp near (0.2,0,0.2) at 4.40 eV and a cp from Δ_3^z - Δ_2^z transitions near (0,0,0.27) at 4.45 eV. Finally we have contributions from Σ_2 - Σ_1 (22 - 33) transitions with a cp near (0.44,0.44,0) at 4.45 eV, Σ_1 - Σ_1 (22 - 33) transitions with a cp near (0.4,0.4,0) at 4.45 eV, 19 - 27 transitions with an M_2 cp near (0.35,0.15,0.3) at 4.48 eV and a series of weaker transitions listed for completeness in Table (V).

The threshold in $\epsilon_2^{\parallel}$ occurs at 1.76 eV and is the result of 24 - 25 transitions around an M_0 cp near (0.4,0.2,0) which are weaker than in the $\epsilon_2^{\perp}$ case. The shoulder starting at 2.32 eV is caused in part by 23 - 25 transitions and 24 - 25 transitions in a region (mostly along z-direction) around an M_0 cp near (0.4,0,0.3) at 2.31 eV and around an M_1 cp near (0.4,0,0.45) at 2.33 eV respectively. Other contributions are from 24 - 26 transitions in a region around U_1^z - U_1^z with an M_0 cp near (0.5,0,0.4) at 2.46 eV and 22 - 25 transitions in a region around Σ_2 - Σ_1 with an M_0 cp near (0.35,0.35,0) at 2.32 eV. The shoulder around 2.80 eV is caused to a large extent by 24 - 26 transitions in a small region around an M_0 cp near (0.1,0.1,0.4) at 2.81 eV and an M_0 cp near (0.2,0.2,0.5) at 2.79 eV. Other strong contributions are from

21 - 25 transitions with an M_0 cp near (0.45,0.15,0.3) at 2.73 eV, $U_1^y - U_1^y$ transitions with an M_1 cp near (0.5,0.2,0) at 2.78 eV and 22 - 26 transitions in a region (along z-direction) around (0.5,0.3,0.15) at 2.82 eV and an M_0 cp at M at about 2.65 eV. Weaker contributions are from $Z_1 - Z_1$ (24 - 27) transitions with an M_0 cp at 2.79 eV and 24 - 25 transitions with an M_2 cp near (0.2,0.05,0.4) at 2.81 eV.

The peak at 3.30 eV is caused in part by 21 - 25 transitions in a region (tubular along z-direction) around U^x with an M_2 cp near (0.2,0,0.5) at 3.33 eV and 23 - 27 transitions with an M_1 cp near (0.35,0.15,0.3) at 3.31 eV. Additional contributions to this peak are from 22 - 26 transitions in a region around what appears to be an M_2 cp near (0.25,0.25,0.3) at 3.36 eV and 23 - 26 transitions in a region near Γ with particularly strong contributions from $\Delta_4^z - \Delta_4^z$ transitions at about 3.3 eV. Finally we have contributions from 24 - 26 transitions with an M_2 cp near (0.12,0.12,0.25) at 3.25 eV and 21 - 28 transitions in a region around $\Sigma_2 - \Sigma_1$ with a cp of undetermined symmetry near (0.4;0.4,0) at 3.3 eV. The peak at 3.65 eV is the result of three main types of contributions. First we have 22 - 27 transitions in a region near Z off the S direction with a probable M_1 cp near (0.15,0.1,0.45) at 3.64 eV along with an M_1 cp near (0.2,0,0.4) at 3.69 eV, and 21, 22 - 27 transitions in a region of relatively large matrix elements near M off the U^x direction with a probable M_0 cp near (0.37,0.1, 0.4) at 3.62 eV and an M_0 cp near (0.3,0.3,0.25) at 3.60 eV. Secondly, we have 19 - 25 transitions, in a region near Z around $S_1 - S_1$, with an M_0 cp near (0.1,0.1,0.5) at 3.65 eV, and 20 - 25 transitions also near Z

but around U^x with an M_0 cp near (0.1,0,0.5) at 3.60 eV and what appears to be an M_0 cp near (0.2,0.1,0.3) at 3.62 eV. Thirdly, we have 24 - 28 transitions, with a cp of undetermined symmetry near $S_1 - S_1$ (0.25,0.25,0.5) at 3.65 eV and a region around $T_1 - T_1$ with an M_3 cp near (0.5,0.21,0.5) at 3.74 eV, and 23 - 28 transitions with an M_1 cp near T at about (0.5,0.15,0.4) at 3.60 eV along with weaker $\Delta_1 - \Delta_2$ (24 - 27) transitions with a cp near (0.35,0,0) at 3.65 eV.

The large peak at 3.90 eV is caused in part by 24 - 30 transitions in a region around an M_1 cp near (0.5,0.22,0.25) at 3.92 eV and 24 - 29,30 transitions in a region around $Z_1^x - Z_1^x$ with an M_0 cp at 3.93 eV and particularly strong contributions along $U_1^y - U_1^y$ at 3.95 eV. Other important contributions are from 24 - 29 transitions in a region with very large matrix elements around $\Gamma_3 - \Gamma_4$ with an M_2 cp at 3.98 eV and 23 - 29 transitions with an M_0 cp near (0.2,0,0.3) at 3.91 eV. Next we have 18 - 25 transitions in a region around (0.3,0,0.4) contributing at 3.90 eV, $\Delta_2 - \Delta_1$ transitions with a cp near (0.35,0,0) also at 3.90eV, and 21 - 26 transitions in a region around $\Sigma_2 - \Sigma_1$ with an M_1 cp near (0.16,0.16,0) at 3.92 eV. Finally we have 22 - 30 transitions with an M_0 cp near (0.35,0.35,0.1) at 3.81 eV and 23 - 28 transitions with a cp near (0,0,0.22) at 3.88 eV.

The shoulder around 4.26 eV is caused in part by 20 - 25 transitions in a region (along z-direction) of large matrix elements around $\Gamma_3 - \Gamma_4$ with an M_0 cp at 4.07 eV, 22 - 29 transitions in a region (along z-direction) around M with a probable M_1 cp at 4.23 eV, and 22 - 32 transitions in a region around $M_3^z - M_3^z$ with a cp at 4.30 eV and in a region around

$U_1^y - U_1^y$ with a cp near (0.5,0.3,0) at 4.26 eV. Additional contributions to this shoulder are from 20 - 28 transitions in a region around (0.4,0.2, 0.25) at 4.30 eV, 18 - 27 transitions in a region around $Z_1 - Z_1$ with an M_1 cp at 4.25 eV and 19 - 25, 26 transitions in a region around (0.25,0.25,0.3) at 4.28 eV. Finally we have 24 - 30 transitions with critical points of undetermined symmetries near $U_1^z - U_1^z$ (0.5,0,0.15) at 4.26 eV, $S_1 - S_1$ (0.3,0.3, 0.5) at 4.27 eV, $\Delta_1 - \Delta_2$ (0.36,0,0) at 4.26 eV and an M_3 cp near (0.3,0.1, 0.2) at 4.41 eV. The last structure we shall consider in the $\epsilon_2^{\parallel}$ spectrum occurs at 4.96 eV. This shoulder is caused in part by 20 - 28, 29 transitions in a region (mostly along z-direction) around (0.3,0,0.25) at 4.95 eV. Other contributions to this shoulder from critical points of undetermined symmetry are listed in Table VI.

IV. Discussion of Amorphous Phases

The experimental amorphous dielectric function $\epsilon_2(E)$[3,4] (Figs. 13 and 14) consists of a seemingly featureless spectrum with one broad peak positioned near the Λ peak in the FC-2 ϵ_2. This spectrum is quite different from any known crystalline ϵ_2 (except for ST-12) and cannot be obtained by simply averaging the peaks in the FC-2 spectrum.

The theoretical attempts[9-14] to explain the amorphous ϵ_2 have all assumed that long range disorder is of primary importance. They have taken the FC-2 band structure as a starting point and have applied various modifications to study the effect of long range disorder. In some cases[9,13] complete k non-conservation was considered in the sense of a non-direct transition (NDT) and in other cases[10-12,14] partial $\vec{k}$ non-conservation was proposed which enabled the introduction of some type of short range order parameter. In all cases, however, the results are similar, in good agreement with experimental ϵ_2 data, and the authors agree that strong $\vec{k}$ non-conservation (long range disorder) is a requisite in explaining the amorphous ϵ_2. None of these theories, however, predicts even a correct <u>trend</u> to the density of states of the amorphous phase. The single broad peak[2] at the bottom of the valence band density of states for the amorphous case is very striking and cannot be accounted for by a simple broadening of the two s-like peaks in the FC-2 structure. This problem was discussed in I where we suggested that the experimental results could be explained by a short range disorder which would make the presence of five and seven fold rings of bonds appreciable. It is precisely the lack of

this short range disorder in these theories that produces this inconsistency with the experimental data. To see this let us examine one of the most interesting and sophisticated of the aforementioned theories, which is that of a complex band structure (CBS)[12,14]. It was instigated by the work of Maschke and Thomas[11] and developed by Kramer. A one electron Green function is expanded in a Born series and a configurational averaging is applied by introducing in each term containing n scattering centers an n-particle correlation function which is integrated over all n sites. It is then assumed that the n-particle correlation functions can be approximated by products of two particle correlation functions which are taken to be sums of Gaussian-like functions centered on lattice sites, with half-widths which increase with increasing distance from a given lattice point and are proportional to a small parameter α which describes the amount of disorder. This type of approximation treats correctly multiple scattering at one atom only while higher multiple scattering terms are treated approximately correctly if one has $\alpha \ll 1$. The two body correlation functions can be related to experimental amorphous radial distribution functions (RDF), however we notice that in Ge for example it would be difficult to reproduce the second and third hump in the RDF[15] curves by simply placing Gaussian-like functions at FC-2 lattice points.

Nevertheless, the averaged Green function series, which is written in terms of pseudopotentials $v(q)$,[16] can be reduced if one assumes slowly varying potential functions and small enough α so as to take $v(q)$ constant in the $\vec{k}$-integration which in turn permits decoupling of terms and a

resummation of the series. The poles of this averaged Green function are now obtained from a generalized pseudopotential secular equation which is now no longer Hermitian. Kramer then finds that he obtains complex energies whose real parts are approximately the energies of the crystal and whose imaginary parts can be interpreted as average reciprocal lifetimes or equivalently average energy widths. The average $\epsilon_2^{\text{spectrum}}$ is obtained by using the Kubo formula and performing a similar configurational averaging on a product of two one electron Green functions. With some approximations the forms for the averaged ϵ_2 and density of states are similar in that they are written as a sum over partial spectra belonging to different regions of the BZ where the reciprocal lifetimes can be taken constant. The partial spectra are then given by a convolution of the crystalline spectrum (shifted in energy when appropriate as shown below) with a Lorentzian which depends on an average reciprocal lifetime. The parameter α was chosen to fit the ϵ_2 spectrum of amorphous Ge and Si.

Kramer's results show the valence band being affected very slightly while the conduction band is broadened considerably. In particular, for Ge the $\Gamma_{25} - \Gamma_2$ and $L_1 - L_3$ gaps become smaller while the $X_4 - X_1$ gap becomes larger. Furthermore, Γ_2 is very slightly broadened, L_2 is slightly broadened, and X_1 is largely broadened. This is not surprising nor difficult to understand. In principle, we would expect the electrons in the conduction band to be affected more by long range disorder than the very well localized valence electrons. In fact, if we look at the charge density at symmetry points in the conduction band, we find that X_1 is

largely spread out while L_3 is somewhat localized and Γ_2 shows definite signs of localization. This is exactly the same trend observed in the reciprocal life times mentioned above. The effect of this on ϵ_2 is then to average out most of the X peak while preserving the Λ peak and shifting it to slightly lower energies. The agreement with the experimental amorphous ϵ_2 is good. The effect of Kramer's disorder on the density of states, however, is a strong averaging of the conduction band and a very small averaging of the valence band peaks for FC-2. This is certainly not in agreement with experiment.[2] The problem is that one is dealing here with a system that has the short range order of diamond. In fact, the parameter α, used to fit ϵ_2, is very small and corresponds, for example, to all first, second and half the third nearest neighbors being within a deviation of only $0.04\underline{a}$ of the crystalline FC-2 positions. It could be suggested that the density of states might agree better with experiment if α was taken to be larger. But now the ϵ_2 would be shifted to lower energies and agreement with experiment here would be considerably marred. Besides, the approximations involved in obtaining Kramer's final expressions may not be valid for large α.

Thus we believe that the conclusions drawn by applying the CBS theory to the FC-2 structure are not valid for the amorphous case. The suggestion[17] that the peak in the amorphous ϵ_2 is due to Λ transitions because of the preservation of the bonding direction is highly questionable and is only a conjecture supported by analyzing a hypothetical "amorphous" system that is too close to the FC-2 structure.

The results from these theories lead us to suspect that the ϵ_2 spectrum

may not be a good judge of the microscopic structural aspects of the amorphous state and that one needs a theory that will be able to account for both the density of states and ϵ_2 in the amorphous phase. In I we applied the concept of short range disorder to the density of states and obtained good agreement with experiment. We shall how do the same for the ϵ_2 spectrum.

There are two features of the amorphous ϵ_2 spectrum which are of primary importance. These are, of course, the one hump form of the spectrum and the position in energy of this hump. We shall attempt to account for these features in the following analysis.

The crystalline $\epsilon_2(E)$ may be written as:

$$\epsilon_2(E) = CJ(E) \sum_{\vec{k}} \sum_{c,v} \delta(E_c(\vec{k}) - E_v(\vec{k}) - E) \left| \langle \psi_c(\vec{k}) | \vec{r} | \psi_v(\vec{k}) \rangle \right|^2 / J(E) \qquad (2)$$

where C is a constant and J(E) is the joint density of states given by:

$$J(E) = \sum_{\vec{k}} \sum_{c,v} \delta(E_c(\vec{k}) - E_v(\vec{k}) - E) \ . \qquad (3)$$

Equation (2) is just an expression for an average matrix element P(E) multiplied by the joint density of states J(E). If we now incorporate the constant C into J(E) we can write:

$$\epsilon_2(E) = J(E)\ P(E) \ . \qquad (4)$$

This is a physically reasonable expression and could be used to study the amorphous phase since it is essentially the number of states accessible for

transitions at an energy E, multiplied by an average probability for those transitions. When one does band structure calculations, however, it is easier to calculate an associated average matrix element M(E) obtained by a weighted averaging of $|\langle\psi_c(\vec{k})|\vec{\nabla}|\psi_v(\vec{k})\rangle|^2$. Then Eq. (3) can be written as:[18]

$$\epsilon_2(E) = J(E) \cdot \frac{M(E)}{E^2} . \qquad (5)$$

Equation (3) or (4) can now be used to qualitatively account for the amorphous ϵ_2 spectrum in a simple way. In the amorphous case we would expect J(E) to be a monotonically increasing function of energy without any sharp structure from specific localized regions in the BZ. Similarly we would expect the average dipole matrix element P(E) to be a smooth monotonically decreasing function of energy. The product of these two functions would then give a one hump structure which would explain the shape of the amorphous ϵ_2. To examine this in more detail we have calculated ϵ_2, J/E^2 and M, and J and M/E^2 as functions of energy for Ge and Si in the FC-2, 2H-4, BC-8 and ST-12 structures using the Gilat-Raubenheimer[8] integration scheme. The results are shown in Figs. 13 and 14. For each row the product of the two curves in the second and third columns gives the ϵ_2 spectrum in the first column. In the cases of 2H-4 and ST-12 structures we show the weighted average of the parallel and perpendicular components of ϵ_2. We are interested in observing the trends as we go from FC-2 down the columns to more and locally disordered and complicated crystal structures. For the moment let us concentrate on the third column in each figure. We notice that with the increasing complexity of the crystal structures, J gradually loses the sharp

structure prominent in the FC-2 case which was caused by the simplicity and symmetry of this band structure. When we reach ST-12, J is almost a smooth and featureless spectrum which would compare well with what we expected in the amorphous case. In addition the average dipole matrix element M/E^2 for ST-12 is for the most part a smooth decreasing function of energy. This is particularly the case for Ge ST-12 in a large energy region while in ST-12 this is true for $E > 3$ eV which, however, contains the peak of ϵ_2. If we now examine the ϵ_2 spectra we notice that it is precisely the ST-12 structure that has the qualities of the superimposed amorphous ϵ_2 spectrum obtained by Donovan and Spicer[3] for Ge and by Pierce and Spicer[4] for Si. The agreement between the ST-12 spectra and the amorphous spectra is quite encouraging and shows that the kind of short range disorder[1] which accounted for the amorphous density of states also accounts for the important features of the amorphous ϵ_2 spectrum. The discrepancy in magnitude of the ϵ_2 curves is irrelevant in this discussion and is caused in part by the differences in bulk density of the ST-12 and amorphous structures.

An interesting feature that comes out of this analysis is that J/E^2 should look something like a step function in the amorphous case since J is such a smooth polynomial-like increasing function of energy. This would then suggest that the average gradient matrix element M must contain most of the information about ϵ_2. This is shown in Figs. 13 and 14 as we go down the second column where we have plotted J/E^2 and M. In the FC-2 case the ϵ_2 spectrum looks mostly like J/E^2 while M simply modulates the J/E^2 spectrum. In the 2H-4 structure we find that the form of the ϵ_2 spectrum

is now shared between J/E^2 and M where M contributes most of the first peak and J/E^2 contributes the second peak. When we examine the BC-8 case we find that the ϵ_2 spectrum now looks mostly like M while J/E^2 just modulates the M spectrum. Finally, in the ST-12 structure we find that J/E^2 is a relatively featureless step-like function of energy and again ϵ_2 looks like M.

Therefore, we can safely conclude from this that the average gradient/matrix element M determines the position in energy of the hump in the amorphous ϵ_2, and most important, when one measures the amorphous ϵ_2 spectrum, one is essentially just measuring the average matrix element M.

V. Conclusions

Our aim in this work has been two-fold. First to make a complete band structure analysis of Ge and Si in a series of novel, interesting and complicated crystal structures. This included calculating energy eigenvalues, densities of states, optical functions, determining the symmetry of wavefunctions and identifying optical structure. Secondly, to use the increasing complexity of the crystal structures to study the trends observed in the density of states and the imaginary part of the dielectric function as we approach the amorphous phase. To this end we have made particular use of the ST-12 structure which has deviations in bond lengths and angles and has odd-numbered rings of bonds. We have not used the ST-12 structure as a replica of amorphous Ge and Si, but rather as a tool to probe the important microscopic structural aspects of the amorphous phase.

We have found that if one is to make a reliable model of the amorphous

phase, one cannot start with a long-range disorder model applied to the FC-2 structure. On the other hand, a short-range disorder model, defined as a system with deviations in bond angles, bond lengths, with all bonds, satisfied and with odd-numbered rings of bonds, could account for both the amorphous density of states and imaginary part of the dielectric function. In particular we found that the amorphous ϵ_2 is just the spectrum of an average matrix element.

If we now include long-range disorder to our short-range disorder, we would expect to have a much better model for the amorphous phase. Our point is, however, that the effects of long-range disorder are of secondary importance.

References

*Supported in part by National Science Foundation Grant GH 35688.

1. J. D. Joannopoulos and M. L. Cohen, Phys. Rev. 1973 (in press).
2. L. Ley, S. Kowalczyk, R. Pollak, and D. A. Shirley, Phys. Rev. Letters 29, 1088 (1972).
3. T. M. Donovan and W. E. Spicer, Phys. Rev. Letters 21, 1572 (1968).
4. D. T. Pierce and W. E. Spicer, Phys. Rev. B5, 3017 (1972).
5. J. S. Kasper and S. M. Richards, Acta. Cryst. 17, 752 (1964).
6. A. W. Luehrmann, Thesis, University of Chicago, 1967.
7. J. Zak, A. Casher, M. Glück, Y. Gur, The Irreducible Representation of Space Groups, ed. J. Zak, W. A. Benjamin, N. Y., 1969.
8. G. Gilat and L. J. Raubenheimer, Phys. Rev. 144, 390 (1966).
9. F. Herman and J. P. Van Dyke, Phys. Rev. Letters 21, 1575 (1968).
10. D. Brust, Phys. Rev. Letters 23, 1232 (1969).
11. K. Maschke and P. Thomas, phys. stat. sol. 39, 453 (1970).
12. B. Kramer, phys. stat. sol. 41, 649 (1970).
13. K. Maschke and P. Thomas, phys. stat. sol. 41, 743 (1970).
14. B. Kramer, phys. stat. sol. 47, 501 (1971).
15. D. E. Sayers, E. A. Stern, and F. W. Lytle, Phys. Rev. Letters 27, 1204 (1971).
16. M. L. Cohen and T. K. Bergstresser, Phys. Rev. 141, 789 (1966).
17. J. Stuke, J. Non.-Cryst. Solids 4, 1 (1970).
18. A similar expression has also been used by Maschke and Thomas (Ref. 13).

Table Captions

Table I Theoretical ϵ_2 structure and identifications, including the location in the BZ, symmetry and energy of critical points for Ge and Si in the 2H-4 structure. Details are given in the text.

Table II Theoretical ϵ_2 structure and identifications, including the location in the BZ, symmetry and energy of critical points for Ge and Si in the BC-8 structure. Details are given in the text.

Table III Theoretical ϵ_2 structure, with perpendicular polarization, and identifications, including the location in the BZ, symmetry and energy of critical points for Ge ST-12. Details are given in the text.

Table IV Theoretical ϵ_2 structure, with parallel polarization, and identifications including the location in the BZ, symmetry and energy of critical points for Ge ST-12. Details are given in the text.

Table V Theoretical ϵ_2 structure, with perpendicular polarization, and identifications, including the location in the BZ, symmetry and energy of critical points for Si ST-12. Details are given in the text.

Table VI Theoretical ϵ_2 structure, with parallel polarization, and identifications, including the location in the BZ, symmetry and energy of critical points for Si ST-12. Details are given in the text.

Figure Captions

Fig. 1. Brillouin zones and associated symmetry points and lines for the 2H-4, BC-8 and ST-12 structures.

Fig. 2 Band structure of Ge in the 2H-4 or wurtzite structure.

Fig. 3 Imaginary part of the dielectric function, ϵ_2, for Ge 2H-4 with parallel (top) and perpendicular (bottom) polarizations.

Fig. 4 Band structure of Si in the 2H-4 or wurtzite structure.

Fig. 5 Imaginary part of the dielectric function, ϵ_2, for Si 2H-4 with parallel (top) and perpendicular (bottom) polarizations.

Fig. 6. Band structure of Ge in the BC-8 structure.

Fig. 7 Imaginary part of the dielectric function, ϵ_2, for Ge BC-8 (top) and Si BC-8 (bottom).

Fig. 8 Band structure of Si in the BC-8 structure.

Fig. 9 Band structure of Ge in the ST-12 structure.

Fig. 10 Imaginary part of the dielectric function, ϵ_2, for Ge ST-12 with parallel (top) and perpendicular (bottom) polarizations.

Fig. 11 Band structure of Si in the ST-12 structure.

Fig. 12 Imaginary part of the dielectric function, ϵ_2, for Si ST-12 with parallel (top) and perpendicular (bottom) polarizations.

Fig. 13 Imaginary part of the dielectric function ϵ_2, average gradient matrix element M, associated joint density of states J/E^2, average dipole matrix element M/E^2, and joint density of states J for Ge in the FC-2, 2H-4, BC-8, and ST-12 structures. For each row the product of the two curves in the second and third columns gives the ϵ_2 spectrum in the first column. The ϵ_2 for the 2H-4 and ST-12 structures was obtained

by averaging over parallel and perpendicular polarizations. The matrix element M is in units of $(\frac{2\pi}{a})^2$ where a is the smallest lattice constant of each crystal and J in the figure is in units of $(\frac{a}{2\pi})^2$ $(eV)^2$. The un-normalized J(E) defined in equation (3) can be obtained from the values of J in the figure by taking J to be in units of $\left(\frac{3\pi m^2}{e^2\hbar^4}\right)\left(\frac{a}{2\pi}\right)^2 \frac{1}{(cm)^3 eV}$. The amorphous ϵ_2 is from Donovan and Spicer (Ref. 3).

Fig. 14 Imaginary part of the dielectric function ϵ_2, associated average matrix element M, associated joint density of states J/E^2, average dipole matrix element M/E^2, and joint density of states J for Si in the FC-2, 2H-4, BC-8, and ST-12 structures. The convention is the same as in Fig. 13. The amorphous ϵ_2 is from Pierce and Spicer (Ref. 4).

TABLE I

Ge 2H-4

ε_2 PEAKS (eV)		BANDS	LOCATION IN ZONE	SYMMETRY	ENERGY (eV)
1.46	⊥	7,8-10	$\Gamma_5 - \Gamma_8$	M_0	1.46
1.77	∥	6-10	$\Gamma_1 - \Gamma_8$	M_0	1.77
2.25	⊥	5-9	$\Gamma_6 - \Gamma_{10}$	M_0	2.08
			$\Delta_6 - \Delta_3$		2.23
		6-9	$A_3 - A_1$	M_1	2.26
2.50	∥	7-9	(0.25, 0, 0.35)	M_0	2.48
2.50	⊥	8-10	$\Delta_5 - \Delta_1$ (0, 0, 0.3)	M_1	2.51
2.68	⊥	8-9	$U_4 - U_2$ (0.5, 0, 0.35)	~ M_1	2.68
2.75	∥	7-9	$U_2 - U_2$ (0.5, 0, 0.4)	M_1	2.78
3.15	∥	7-10	(0.08, 0.08, 0.2)	M_0	3.03
		7-9	(0.11, 0.11, 0.2)	~ M_2	3.14
3.35	⊥	6-9	(0.2, 0, 0.25)	M_1	3.35
3.57	∥	8-9	(0.2, 0.2, 0.35)	~ M_1	3.57
3.60	⊥	6-9	$M_7 - M_1$		3.61
			$\Sigma_4 - \Sigma_1$		3.59
			$U_3 - U_1$ (0.5, 0, 0.15)	~ M_2	3.60
		8-10	(0.2, 0, 0.4)	M_2	3.80
			$R_2 - R_1$ (0.25, 0, 0.5)		3.60
3.72	∥	8-9	(0.3, 0.3, 0.45)	M_1	3.72
4.52	⊥	8-11	$L_2 - L_1$, $U_4 - U_2$	~ M_0	4.40
		8-9	T (0.23, 0.23, 0)	~ M_0	4.45
		7-11	(0.25, 0, 0.25)	~ M_1	4.53
4.52	∥	7-11	(0.25, 0, 0.25)	~ M_1	4.53
		8-9	K, T'	M_2	4.52
4.70	⊥	7-9	K, T'	~ M_2	4.67
		8-9	(0.4, 0.15, 0.15)	M_3	4.72
		8-12	$A_3 - A_3$, $S_1 - S_1$ (0.03, 0.03, 0.45)	~ M_2	4.71
4.70	∥	8-11	M, T'	M_0	4.67
		7-9	K, P (0.33, 0.33, 0.15)	~ M_3	4.90
5.23	⊥	8-14	$\Gamma_5 - \Gamma_{12}$	M_2	5.23
		8-11	(0.08, 0.08, 0.35)	M_3	5.30
5.29	∥	8-12	$M_5 - M_4$		5.33
			$\Sigma_3 - \Sigma_4$		5.31

Si 2H-4

ε_2 PEAKS (eV)		BANDS	LOCATION IN ZONE	SYMMETRY	ENERGY
2.60	⊥	7-9	$\Sigma_1 - \Sigma_1$ (0.3, 0, 0)	M_0	2.60
2.60	∥	7-9	$\Sigma_1 - \Sigma_1$		2.60
3.10	∥	7-9	(0.25, 0, 0.25)	M_0	3.02
3.35	∥	7-9	$U_2 - U_2$ (0.5, 0, 0.35)	M_1	3.34
3.35	⊥	5-9	$\Gamma_6 - \Gamma_{10}$	M_0	3.21
			$\Delta_6 - \Delta_3$		3.31
		6-9	$A_3 - A_1$	M_1	3.35
3.60	⊥	8-10	$\Delta_5 - \Delta_1$ (0, 0, 0.25)	M_1	3.59
4.10	⊥	6-9	$M_7 - M_1$		4.08
			$\Sigma_4 - \Sigma_1$		4.09
			$U_3 - U_1$ (0.5, 0, 0.25)	M_2	4.11
		7-9	$R_2 - R_1$ (0.15, 0, 0.5)	M_2	4.13
4.25	∥	8-9	(0.2, 0.2, 0.35)	~ M_1	4.21
			H, S'		4.26
4.38	⊥	8-10	(0.2, 0, 0.4)	M_2	4.38
			$R_2 - R_1$ (0.2, 0, 0.5)		4.30
4.68	∥	8-10	M, T'	~ M_2	4.64
		8-9	(0.3, 0.1, 0)	M_1	4.68
		7-11	(0.4, 0, 0.35)	M_0	4.61
		7-9	T (0.2, 0.2, 0)	~ M_2	4.74
4.69	⊥	8-9	T (0.2, 0.2, 0)	M_0	4.57
		5,6-10	$\Delta_6 - \Delta_5$ (0, 0, 0.3)	~ M_1	4.69
4.89	⊥	7-9	K	~ M_2	4.87
		8-9	(0.3, 0.25, 0.25)	~ M_2	4.89
4.91	∥	7-10	Σ (0.2, 0.08, 0)	~ M_2	4.91
		8-10	(0.2, 0.1, 0)	~ M_2	4.93
4.96	⊥	8-11	Σ (0.35, 0.05, 0.05)	~ M_2	4.96
5.50	⊥	8-14	$\Gamma_5 - \Gamma_{12}$	M_1	5.47
5.55	∥	8-12	$M_5 - M_4$		5.61
			$\Sigma_3 - \Sigma_4$		5.54

TABLE II

Ge BC-8					Si BC-8				
ε_2 PEAKS (eV)	BANDS	LOCATION IN ZONE	SYMMETRY	ENERGY (eV)	ε_2 PEAKS (eV)	BANDS	LOCATION IN ZONE	SYMMETRY	ENERGY(
2.03	16 - 17	$\Sigma_1 - \Sigma_2$ (0.37, 0.37, 0)	M_1	2.03	0.43	15,16-17	$H_3 - H_4$	M_0	0.43
2.46	15 - 17	$\Sigma_2 - \Sigma_2$ (0.4, 0.4, 0)		2.46	1.70	16-17	$\Delta_1 - \Delta_4$ (0.55, 0, 0)	M_0	1.65
	13 - 17	$\Delta_4 - \Delta_4$ (0.56, 0, 0)	M_0	2.41	2.04	16-17	(0.3, 0.55, 0)	~ M_2	2.04
2.70	13 - 17	(0.2, 0.8, 0.15)	M_0	2.67	2.60	16-18	$\Sigma_1 - \Sigma_2$ (0.4, 0.4, 0)	M_2	2.62
	14 - 18	$G_2 - G_1$ (0.15, 0.85, 0)	~ M_0	2.65		15-17	(0.3, 0.5, 0)	M_0	2.54
3.21	16 - 19	(0.25, 0.35, 0.25)	M_0	3.19	3.00	13-17	(0.2, 0.7, 0.15)	M_0	2.96
	13 - 17	$G_1 - G_2$ (0.4, 0.6, 0)	M_2	3.24	3.45	13-17	(0.1, 0.5, 0.1)		3.46
		(0.3, 0.4, 0.15)		3.23		14-17	(0.2, 0.4, 0.15)	~ M_2	3.45
	14 - 17	(0.2, 0.4, 0.15)	~ M_2	3.21		16-19	(0.3, 0.4, 0.2)	M_1	3.43
	13 - 18	(0.3, 0.45, 0)	M_1	3.21		16-17	$\Gamma_1 - \Gamma_6$	M_0	3.38
		$G_1 - G_1$ (0.22, 0.78, 0)		3.23	3.70	13-17	$G_1 - G_2$ (0.45, 0.55, 0)	M_2	3.70
3.76	15 - 19	$N, G_2 - G_1$ (0.4, 0.55, 0)	M_3	3.78		15-19	$D_1 - D_1$ (0.5, 0.5, 0.15)	M_1	3.68
	12 - 18	$G_2 - G_1$ (0.35, 0.65, 0)	M_1	3.76	4.05	16-21	(0.2, 0.6, 0.15)		4.05
	15-17,18	$\Gamma_2 - \Gamma_6$	M_3	3.74			$\Delta_1 - \Delta_2$ (0.5, 0, 0)	M_2	4.04
3.98	14-19	(0.25, 0.65, 0.15)		4.00		15-21	(0.2, 0.6, 0.1)	M_0	4.02
4.50	12-19	(0.26, 0.63, 0.15)		4.50		13-18	$G_1 - G_1$ (0.2, 0.8, 0)		4.02
	16-21	(0.15, 0.2, 0.1)	M_2	4.48		14-19	(0.25, 0.65, 0.1)	~ M_1	4.07
	14-20	(0.1, 0.5, 0.1)		4.50	4.20	16-22	(0.2, 0.5, 0)	~ M_2	4.20
	15-19	$\Delta_1 - \Delta_4$ (0.25, 0, 0)	M_0	4.42		12-18	(0.15, 0.7, 0.15)	M_2	4.22
						15-22	(0.15, 0.7, 0)	M_0	4.14
					5.05	14-21	(0.2, 0.6, 0.1)	M_2	5.05
						13-20	$D_1 - D_1$ (0.5, 0.5, 0.1)		5.00

TABLE III

Ge ST-12 $\vec{E} \perp \vec{c}$

ϵ_2 PEAKS (eV)	BANDS	LOCATION IN ZONE	SYMMETRY	ENERGY (eV)
1.46	23,24 - 25	$\Sigma_1 - \Sigma_1$ (0.35, 0.35, 0)	M_0	1.46
2.10	24 - 25	(0.4, 0.1, 0.3)	$\sim M_0$	2.08
	23 - 25	(0.4, 0, 0.3)	M_1	2.18
2.55	24 - 26	(0.5, 0.1, 0.3)	M_1	2.48
		$T_1 - T_1$ (0.5, 0.5, 0.4)		2.52
		$U_1^z - U_1^z$ (0.5, 0, 0.3)		2.50
	23 - 26	(0.4, 0.15, 0.25)		2.62
	22 - 25	(0.4, 0, 0.25)	$\sim M_2$	2.62
		M		2.60
	21 - 25	(0.4, 0.15, 0.25)	M_1	2.60
	24 - 25	(0.1, 0.1, 0.4)	M_0	2.54
2.80	23,24 - 26	$S_1 - S_1$ (0.4, 0.4, 0.5)	M_2	2.87
	21 - 25	(0.4, 0.15, 0.25)	M_1	2.60
		$\Delta_1 - \Delta_1$ (0.4, 0, 0)		2.80
	24 - 25	U^x (0.2, 0, 0.4)	M_1	2.70
	24 - 27	(0.5, 0.1, 0.3)	M_1	2.76
		$\Gamma_3 - \Gamma_5$	M_0	2.75
3.00	20 - 25	(0.4, 0.15, 0.25)	M_0	2.93
	22 - 25	$Z_2 - Z_2$	M_0	2.98
		$T_1 - T_1$ (0.5, 0.5, 0.3)		3.00
	24 - 27	T^z (0.5, 0.5, 0.45)	M_1	3.11
	19 - 25	(0.35, 0.18, 0)		2.97
		$M_2^z - M_1^z$	$\sim M_2$	3.00
	22 - 27	(0.5, 0.15, 0.3)	M_0	3.04
3.20	24 - 27	$Z_1 - Z_1$	M_0	3.18
		$Z_1^x - Z_1^x$	M_3	3.20
	21 - 25	U^x (0.2, 0, 0.5)	M_2	3.21
	23 - 28	R, T^z	$\sim M_1$	3.20
	19 - 25	(0.5, 0.15, 0.3)	M_2	3.21
		$\Delta_1 - \Delta_1$ (0.38, 0, 0)		3.20
3.50	19 - 25, 26	$R_1 - R_1$	M_0	3.46
	19 - 25	$T_1 - T_1$ (0.5, 0.22, 0.5)	$\sim M_0$	3.49
	20 - 25	$S_1 - S_1$ (0.06, 0.06, 0.5)	M_0	3.4
		$S_1 - S_1$ (0.45, 0.45, 0.5)	$\sim M_1$	3.46
	17 - 25	T^z (0.5, 0.5, 0.3)	$\sim M_1$	3.5?
	24 - 27	(0, 0.1, 0.25)	$\sim M_2$	3.47
		$T_1 - T_1$ (0.5, 0.3, 0.5)		3.5(
	20 - 26	$T_1 - T_1$ (0.5, 0.35, 0.5)	M_2	3.4'
	22 - 27	(0.3, 0.1, 0.3)	M_2	3.5'
		$\Delta_1 - \Delta_1$ (0.45, 0, 0)		3.5(
3.65	17 - 25	(0.5, 0.25, 0.3)	M_2	3.6'
		$Z_1 - Z_2$	M_0	3.65
	23 - 27	(0.1, 0, 0.25)		3.65
	24 - 29	U^x (0.22, 0, 0.5)	M_0	3.6(
	24 - 30	$R_1 - R_1$	M_1	3.6(
4.20	24 - 30	U^x (0.3, 0, 0.4)		4.18
		M		4.20
	21 - 27	(0.15, 0.15, 0.2)	M_2	4.22
	23 - 28	$\Delta_2 - \Delta_1$ (0.1, 0, 0.05)		4.2(
	21 - 28	U^x (0.15, 0, 0.4)		4.2(
	20 - 25	$\Sigma_2 - \Sigma_1$ (0.07, 0.07, 0)	M_1	4.21
	23 - 32	$S_1 - S_1$ (0.22, 0.22, 0.5)		4.2(
4.50	23 - 31	$U_1^z - U_1^z$ (0.5, 0, 0.2)	$\sim M_3$	4.57
	21 - 33	$\Sigma_2 - \Sigma_1$ (0.4, 0.4, 0)		4.4'
	22 - 30	U^y (0.45, 0.1, 0.05)	M_1	4.3(
		(0.3, 0.15, 0.4)	M_1	4.5
	20 - 26	(0.15, 0, 0.1)	M_3	4.5'
	20 - 28	(0.15, 0.15, 0.25)	M_0	4.4'
	19 - 27	$M_3^z - M_1^z$		4.4
	23 - 34	$\Sigma_1 - \Sigma_1$ (0.36, 0.36, 0)		4.4'
	23 - 35	$\Sigma_1 - \Sigma_2$ (0.35, 0.35, 0)		4.4'
	21 - 29	$\Delta_3^z - \Delta_1^z$ (0, 0, 0.22)		4.5
	22 - 31	$\Delta_1^z - \Delta_4^z$ (0, 0, 0.3)		4.5
	24 - 33	$U_1^y - U_1^y$ (0.5, 0.2, 0)		4.5

TABLE IV

Ge ST-12 $\vec{E} \parallel \vec{c}$

ϵ_2 PEAKS (eV)	BANDS	LOCATION IN ZONE	SYMMETRY	ENERGY (eV)
1.60	24-25	$\Sigma_2 - \Sigma_1$ (0.35, 0.35, 0)	M_0	1.46
		$\Delta_2 - \Delta_1$ (0.4, 0, 0)	$\sim M_1$	1.90
2.15	21-25	$\Sigma_2 - \Sigma_1$ (0.37, 0.37, 0)	M_0	2.07
	24-25	(0.4, 0.1, 0.3)	$\sim M_0$	2.08
	23-25	(0.4, 0, 0.3)	M_1	2.18
2.65	21-25	(0.4, 0.15, 0.25)	M_1	2.60
		$Z_1^X - Z_1^X$	$\sim M_2$	2.65
		$U_1^Y - U_1^Y$		2.63
	22-26	(0.5, 0.2, 0.25)	M_1	2.74
	22-25	$M_3^Z - M_1^Z$	$\sim M_2$	2.70
	24-25	$\Gamma_3 - \Gamma_4$	M_0	2.64
3.20	24-27	$Z_1 - Z_1$	M_0	3.18
		$Z_1^X - Z_1^X$	M_3	3.20
		$\Delta_2 - \Delta_1$ (0.45, 0, 0)	$\sim M_2$	3.18
	21-25	U^X (0.2, 0, 0.5)	M_2	3.21
		(0.2, 0.2, 0.3)		3.20
	24-26	$S_1 - S_1$ (0.26, 0.26, 0.5)	M_3	3.26
	23-28	$R_1 - R_1$		3.20
	24-28	$\Sigma_2 - \Sigma_1$ (0.25, 0.25, 0)	$\sim M_1$	3.20
3.50	20-25	$Z_2 - Z_2$		3.48
		$S_1 - S_1$ (0.06, 0.06, 0.5)	M_0	3.45
	22-27	(0.3, 0.1, 0.3)	M_2	3.54
		$\Gamma_5 - \Gamma_5$	M_0	3.44
	20-26	(0.3, 0.1, 0.3)		3.53
	24-29	$\Sigma_2 - \Sigma_1$ (0.35, 0.35, 0)		3.45
	24-26	$\Delta_1 - \Delta_2$ (0.3, 0, 0)		3.48
3.70	24-28	$\Delta_1 - \Delta_2$ (0.26, 0, 0)		3.70
		$S_1 - S_1$ (0.2, 0, 0)	$\sim M_2$	3.70
	21-27	$Z_1^X - Z_1^X$	M_1	3.69

ϵ_2 PEAKS (eV)	BANDS	LOCATION IN ZONE	SYMMETRY	ENERGY
		$U_1^Z - U_1^Z$ (0.5, 0, 0.2)		3.71
3.90	19-25	(0.2, 0.15, 0.3)	M_3	3.92
	24-29	$\Delta_2^R - \Delta_2^Z$ (0, 0, 0.18)	M_2	3.94
	23-29	$\Delta_1 - \Delta_2$ (0.37, 0, 0)	$\sim M_2$	3.90
		$S_1 - S_1$ (0.26, 0.26, 0.5)		3.90
	21-26	$\Delta_2 - \Delta_1$ (0.15, 0, 0)	$\sim M_1$	3.88
4.20	24-29	$\Gamma_3 - \Gamma_4$	M_3	4.22
	20-25	$\Gamma_3 - \Gamma_4$	M_0	4.16
		$\Sigma_2 - \Sigma_1$ (0.07, 0.07, 0)	M_1	4.21
	21-28	$\Gamma_2 - \Gamma_1$	M_0	4.22
		$\Delta_1^Z - \Delta_1^Z$		4.23
		U^X (0.15, 0, 0.4)		4.20
		$S_1 - S_1$ (0.25, 0.25, 0.5)		4.20
	22-29	(0.15, 0.15, 0.2)	M_0	4.21
		$Z_1^X - Z_1^X$	M_2	4.24
	24-30	(0.1, 0.1, 0.3)	M_1	4.26
	22-30	(0.3, 0.25, 0.25)		4.21
4.40	20-26	(0.17, 0.17, 0.1)	M_2	4.42
	18-27	$Z_1 - Z_1$	M_0	4.36
	23-28	$\Sigma_2 - \Sigma_1$ (0.14, 0.14, 0)		4.40
	22-27	$\Sigma_1 - \Sigma_2$ (0.14, 0.14, 0)		4.37
		$\Delta_1 - \Delta_2$ (0.25, 0, 0)		4.40
	23-34	$M_2^Z - M_1^Z$	$\sim M_2$	4.40
		$S_1 - S_2$ (0.35, 0.35, 0)		4.40
	16-26	$Z_2 - Z_2$	$\sim M_1$	4.37
		$\Delta_2^R - \Delta_3^R$		4.40
	28-30	(0.35, 0.15, 0.3)	M_3	4.42
		$\Delta_1 - \Delta_2$ (0.37, 0, 0)		4.40
	22-31	$U_1^Y - U_1^Y$ (0.5, 0.3, 0)		4.40

TABLE V

Si ST-12 $\vec{E} \perp \vec{c}$

ϵ_2 PEAKS (eV)	BANDS	LOCATION IN ZONE	SYMMETRY	ENERGY (eV)
1.76	24 - 25	(0.4, 0.2, 0)	M_0	1.76
2.33	23 - 25	(0.4, 0, 0.3)	M_0	2.31
	24 - 25	(0.4, 0, 0.45)	M_1	2.33
2.50	23,24 - 26	M	$\sim M_1$	2.50
		$T_1 - T_1$ (0.5, 0.15, 0.5)	M_1	2.52
		$U_1^z - U_1^z$		2.51
		Z^x, $U_1^y - U_1^y$		2.45
2.80	23,24 - 26	$S_1 - S_1$ (0.4, 0.4, 0.5)		2.76
		(0.4, 0.4, 0.4)	M_1	2.80
	21 - 25	(0.45, 0.15, 0.3)	M_0	2.73
		$\Delta_2 - \Delta_1$ (0.45, 0, 0)		2.80
	21 - 25 }	$U_1^y - U_1^y$ (0.5, 0.2, 0)	M_1	2.79
	22 - 26 }	(0.5, 0.3, 0.15)		2.82
	23 - 28	$Z_1 - Z_1$	M_0	2.78
	22 - 25	(0.4, 0, 0.25)	M_2	2.74
3.20	20 - 25	$\Delta_1 - \Delta_1$ (0.39, 0, 0)	M_0	3.17
		$\Sigma_1 - \Sigma_1$ (0.37, 0.37, 0)	M_2	3.21
	19 - 25	$\Sigma_2 - \Sigma_2$ (0.4, 0.4, 0)	$\sim M_1$	3.18
	22 - 25	$Z_2 - Z_2$	M_0	3.18
		(0.2, 0.2, 0.25)	M_1	3.16
	20 - 26	U^x (0.5, 0.35, 0.05)	M_1	3.17
		$\Sigma_1 - \Sigma_1$ (0.4, 0.4, 0)		3.20
	22 - 28	$U_1^y - U_1^y$ (0.5, 0.4, 0)		3.20
		$R_1 - R_1$		3.20
	21 - 26	T^z (0.5, 0.5, 0.4)	M_2	3.23
3.38	20 - 25	R, T^z (0.5, 0.5, 0.45)	M_1	3.39
	19 - 25	R, T^z (0.48, 0.48, 0.4)	$\sim M_3$	3.45
		$S_1 - \Sigma_1$ (0.35, 0.35, 0)		3.35
	22 - 26	(0.25, 0.25, 0.3)	$\sim M_2$	3.36
	18 - 25	(0.4, 0.2, 0)	M_0	3.35
		$U_1^y - U_1^y$ (0.5, 0.39, 0)		3.40
	24 - 27	(0.15, 0, 0.3)	M_1	3.38
		$U_1^z - U_1^z$ (0.5, 0, 0.15)		3.38
	22 - 28	$Z_2 - Z_1$	M_0	3.37
		(0.45, 0.4, 0.3)	M_1	3.35

ϵ_2 PEAKS (eV)	BANDS	LOCATION IN ZONE	SYMMETRY	ENERGY (eV)
3.60	20 - 25	Z, U^x (0.1, 0, 0.5)	M_0	3.60
	21 - 26	(0.3, 0.2, 0.25)	$\sim M_1$	3.60
	22 - 27	$\Sigma_2 - \Sigma_1$ (0.3, 0.3, 0)	M_0	3.50
	21 - 29	$R_1 - R_1$	M_0	3.59
	23 - 27	(0.1, 0.1, 0.25)	M_0	3.54
	23 - 28	(0.5, 0.15, 0.3)	M_1	3.58
	22 - 26	$\Delta_2^z - \Delta_4^z$ (0, 0, 0.3)		3.60
	22 - 28	$\Sigma_2 - \Sigma_1$ (0.32, 0.12, 0)		3.60
3.85	24 - 29	$Z_1^x - Z_1^x$	M_1	3.92
	23 - 28	$\Gamma_5 - \Gamma_1$	M_0	3.71
		$\Delta_4^z - \Delta_1^z$ (0, 0, 0.24)	M_2	3.85
	23 - 29	(0.35, 0.15, 0.25)		3.85
	17 - 25	$U_1^z - U_1^z$ (0.5, 0, 0.33)		3.85
	22 - 27	(0.15, 0.15, 0.2)	$\sim M_1$	3.81
	21 - 29	$\Sigma_1 - \Sigma_2$ (0.42, 0.42, 0)	M_1	3.88
	20 - 26	(0.15, 0.1, 0.4)	$\sim M_1$	3.89
	16 - 25	$M_3^z - M_2^z$	M_1	3.86
	23 - 30	(0.35, 0.35, 0.25)	$\sim M_1$	3.81
4.45	20 - 26	(0.1, 0, 0.1)	$\sim M_2$	4.48
		$\Sigma_1 - \Sigma_1$ (0.12, 0.12, 0)		4.44
	23 - 35	$M_2^z - M_3^z$		4.46
	15 - 27 }	$M_3^z - M_4^z$	$\sim M_1$	4.45
	15 - 26 }	$\Sigma_2 - \Sigma_1$ (0.44, 0.44, 0)		4.42
		$U_1^z - U_1^z$ (0.5, 0, 0.34)		4.45
	14 - 26	$M_3^z - M_2^z$		4.41
		$T_1 - T_1$ (0.5, 0.28, 0.5)		4.45
	21 - 27	(0.2, 0, 0.2)	$\sim M_1$	4.40
		$\Delta_3^z - \Delta_2^z$ (0, 0, 0.27)		4.45
	22 - 33	$\Sigma_2 - \Sigma_1$ (0.44, 0.44, 0)		4.45
		$\Sigma_1 - \Sigma_1$ (0.4, 0.4, 0)		4.45
	19 - 27	(0.35, 0.15, 0.3)	M_2	4.48
	21 - 28	$\Delta_3^z - \Delta_1^z$ (0, 0, 0.24)		4.43
	22 - 29	$U_1^y - U_1^y$ (0.5, 0.11, 0)		4.41
	19 - 25	$\Sigma_2 - \Sigma_1$ (0.15, 0.15, 0)		4.45
	17 - 29	M		4.42

TABLE VI

Si ST-12 $\vec{E} \parallel \vec{z}$

ϵ_2 PEAKS (eV)	BANDS	LOCATION IN ZONE	SYMMETRY	ENERGY (eV)
1.76	24-25	(0.4, 0.2, 0)	M_0	1.76
2.32	23-25	(0.4, 0, 0.3)	M_0	2.31
	24-25	(0.4, 0, 0.45)	M_1	2.33
	24-26	U_1^z-U_1^t (0.5, 0, 0.4)	M_0	2.46
	22-25	Σ_2-Σ_1 (0.35, 0.35, 0)	M_0	2.32
2.80	24-26	(0.1, 0.1, 0.4)	M_0	2.81
		(0.2, 0.2, 0.5)	M_0	2.79
	21-25	(0.45, 0.15, 0.3)	M_0	2.73
	21-25	U_1^x-U_1^y (0.5, 0.2, 0)	M_1	2.78
	22-26	(0.5, 0.3, 0.15)		2.82
		M	M_0	2.65
	24-27	Z_1 - Z_1	M_0	2.79
	24-25	(0.2, 0.05, 0.4)	M_2	2.81
3.30	21-25	U^x (0.2, 0, 0.5)	M_2	3.33
	23-27	(0.35, 0.15, 0.3)	M_1	3.31
	22-26	(0.25, 0.25, 0.3)	~ M_2	3.36
	23-26	Γ, Δ_4^z - Δ_4^z		3.30
	24-26	(0.12, 0.12, 0.25)	M_2	3.25
	21-28	Σ_2-Σ_1 (0.4, 0.4, 0)		3.30
3.65	22-27	Z, S (0.15, 0.1, 0.45)	~ M_1	3.64
		(0.2, 0, 0.4)	~ M_1	3.69
	21,22-27	M, U^x (0.37, 0.1, 0.4)	~ M_0	3.62
	21-27	(0.3, 0.3, 0.25)	M_0	3.60
	19-25	Z, S_1-S_1 (0.1, 0.1, 0.5)	M_0	3.65
	20-25	Z, U^x (0.1, 0, 0.5)	M_0	3.60
		(0.2, 0.1, 0.3)	~ M_0	3.62
	24-28	S_1-S_1 (0.25, 0.25, 0.3)		3.65
		T_1-T_1 (0.5, 0.21, 0.5)	M_3	3.74
	23-28	T (0.5, 0.15, 0.4)	M_1	3.60
	24-27	Δ_1-Δ_2 (0.35, 0, 0)		3.65

ϵ_2 PEAKS (eV)	BANDS	LOCATION IN ZONE	SYMMETRY	ENERGY (eV)
3.90	24-30	(0.5, 0.22, 0.25)	M_1	3.92
	24-29,30	Z_1^x - t_1^x	M_0	3.93
		U_1^y - U_1^y		3.95
	24-29	Γ_3 - Γ_4	M_2	3.98
	23-29	(0.2, 0, 0.3)	M_0	3.91
	18-25	(0.3, 0, 0.4)		3.90
		Δ_2-Δ_1 (0.35, 0, 0)		3.90
	21-26	Σ_2-Σ_1 (0.16, 0.16, 0)	M_1	3.92
	22-30	(0.35, 0.35, 0.1)	M_0	3.91
	23-28	Δ_2^z-Δ_2^z (0, 0, 0.22)		3.89
4.26	20-25	Γ_3 - Γ_4	M_0	4.07
	22-29	M	~ M_1	4.28
	22-32	M_3^z - M_3^t		4.30
		U_1^y-U_1^y (0.5, 0.3, 0)		4.26
	20-28	(0.4, 0.2, 0.25)		4.80
	18-27	Z_1 - Z_1	M_1	4.25
	24-30	U_1^t-U_1^t (0.5, 0, 0.15)		4.26
		S_1-S_1 (0.3, 0.3, 0.5)		4.27
		Δ_1-Δ_2 (0.36, 0, 0)		4.26
		(0.3, 0.1, 0.2)	M_3	4.41
	19-25,26	(0.25, 0.25, 0.3)		4.28
4.96	20-28,29	(0.3, 0, 0.25)		4.95
	20-28	U_1^t-U_1^t (0.5, 0, 0.2)		4.96
	19-33	Σ_2-Σ_1 (0.43, 0.43, 0)		4.94
	19-26	Δ_2-Δ_1 (0.18, 0, 0)		4.95
	21-29	S_1-S_1 (0.3, 0.3, 0.5)		4.98
		U_1^t-U_1^t (0.5, 0, 0.2)		4.96
	17-31	Σ_2-Σ_1 (0.42, 0.42, 0)		4.97
	23-33	U_1^t-U_1^t (0.5, 0, 0.25)		4.96
	22-31	Σ_2-Σ_1 (0.18, 0.18, 0)		4.94

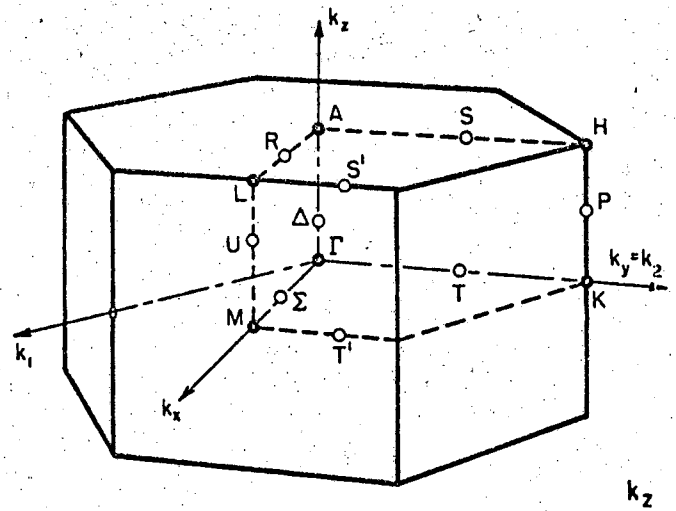

HEXAGONAL

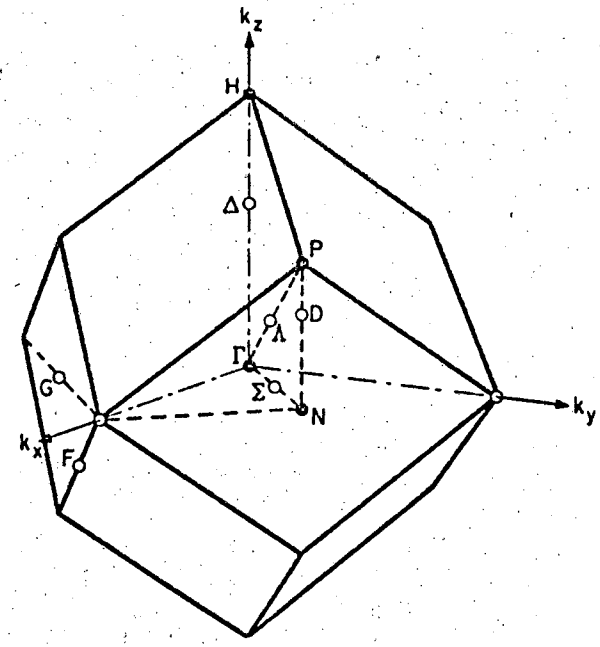

BODY-CENTERED CUBIC

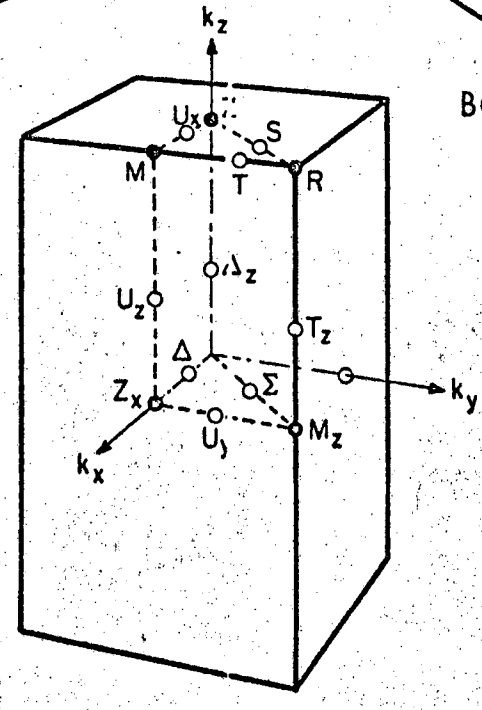

SIMPLE TETRAGONAL

Fig. 1

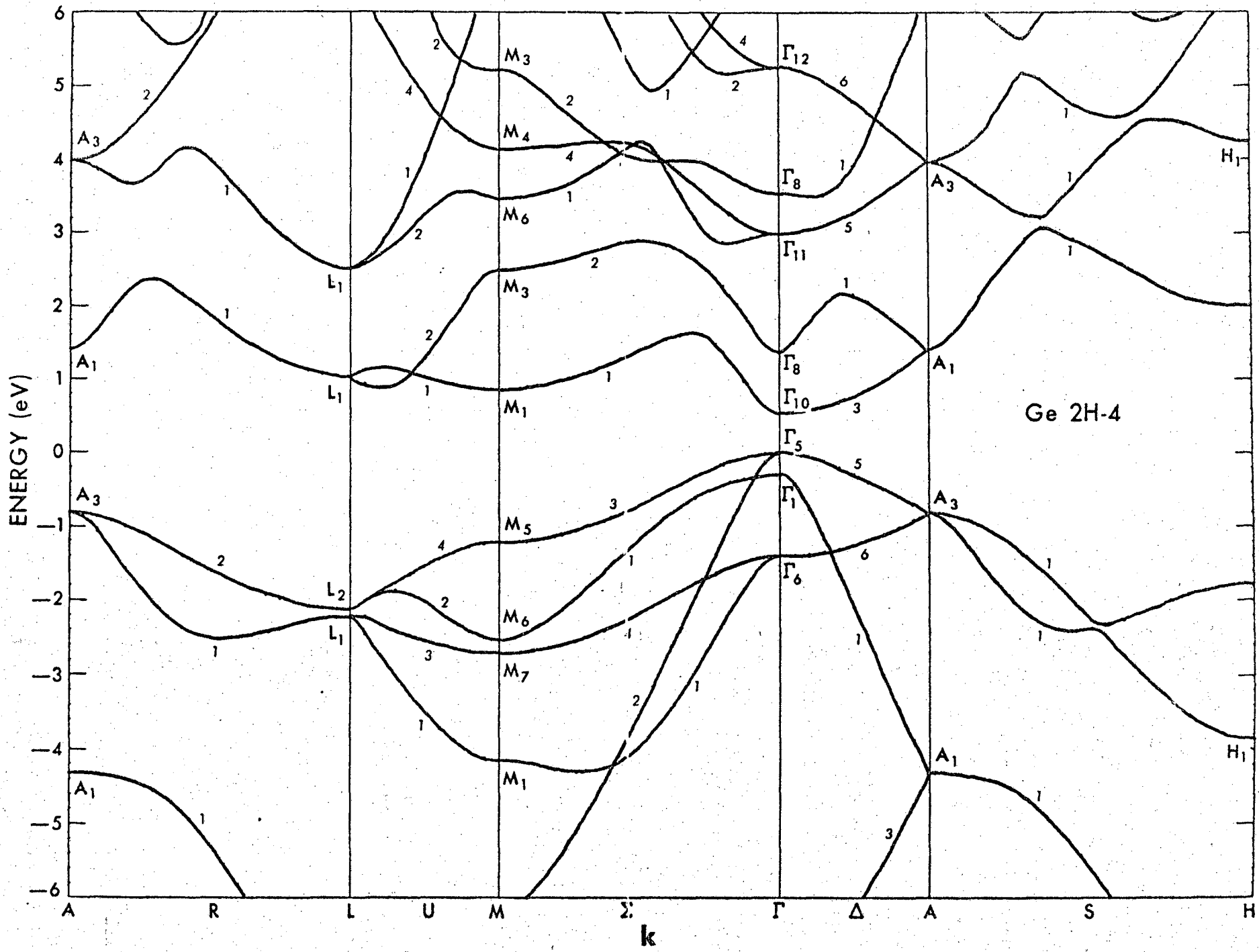
ENERGY (eV)
6
5
4
3
2
1
0
−1
−2
−3
−4
−5
−6
A
R
L
U
M
Σ
Γ
Δ
A
S
H
k
A3
A1
L1
L2
M3
M4
M6
M1
M5
M7
Γ12
Γ8
Γ11
Γ10
Γ5
Γ1
Γ6
H1
Ge 2H-4

Fig 2.

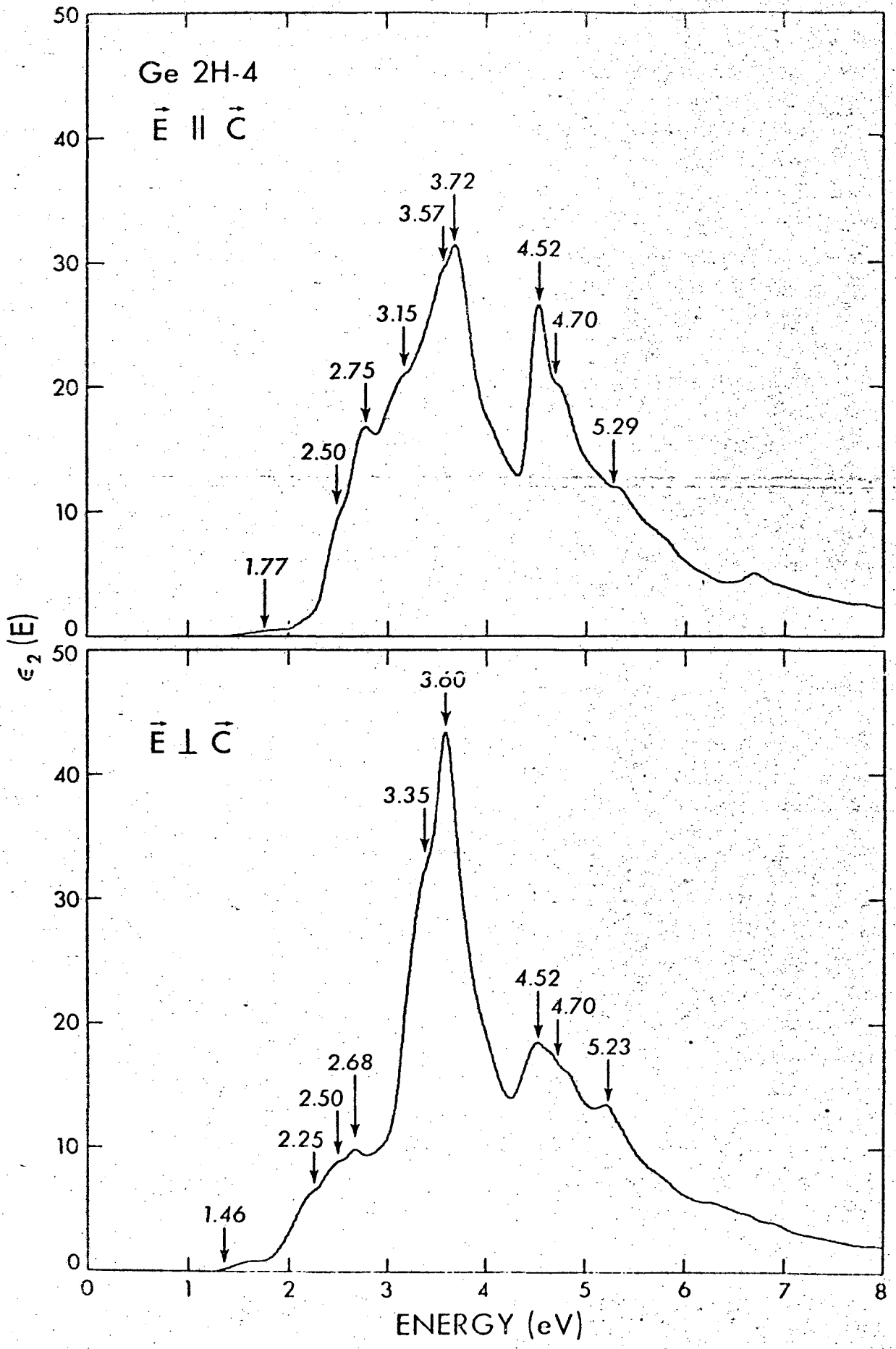
Ge 2H-4
$\vec{E} \parallel \vec{C}$
3.72
3.57
4.52
3.15
4.70
2.75
5.29
2.50
1.77
$\vec{E} \perp \vec{C}$
3.60
3.35
4.52
4.70
5.23
2.68
2.50
2.25
1.46
$\epsilon_2(E)$
ENERGY (eV)
0
10
20
30
40
50
0
1
2
3
4
5
6
7
8

Fig. 3.

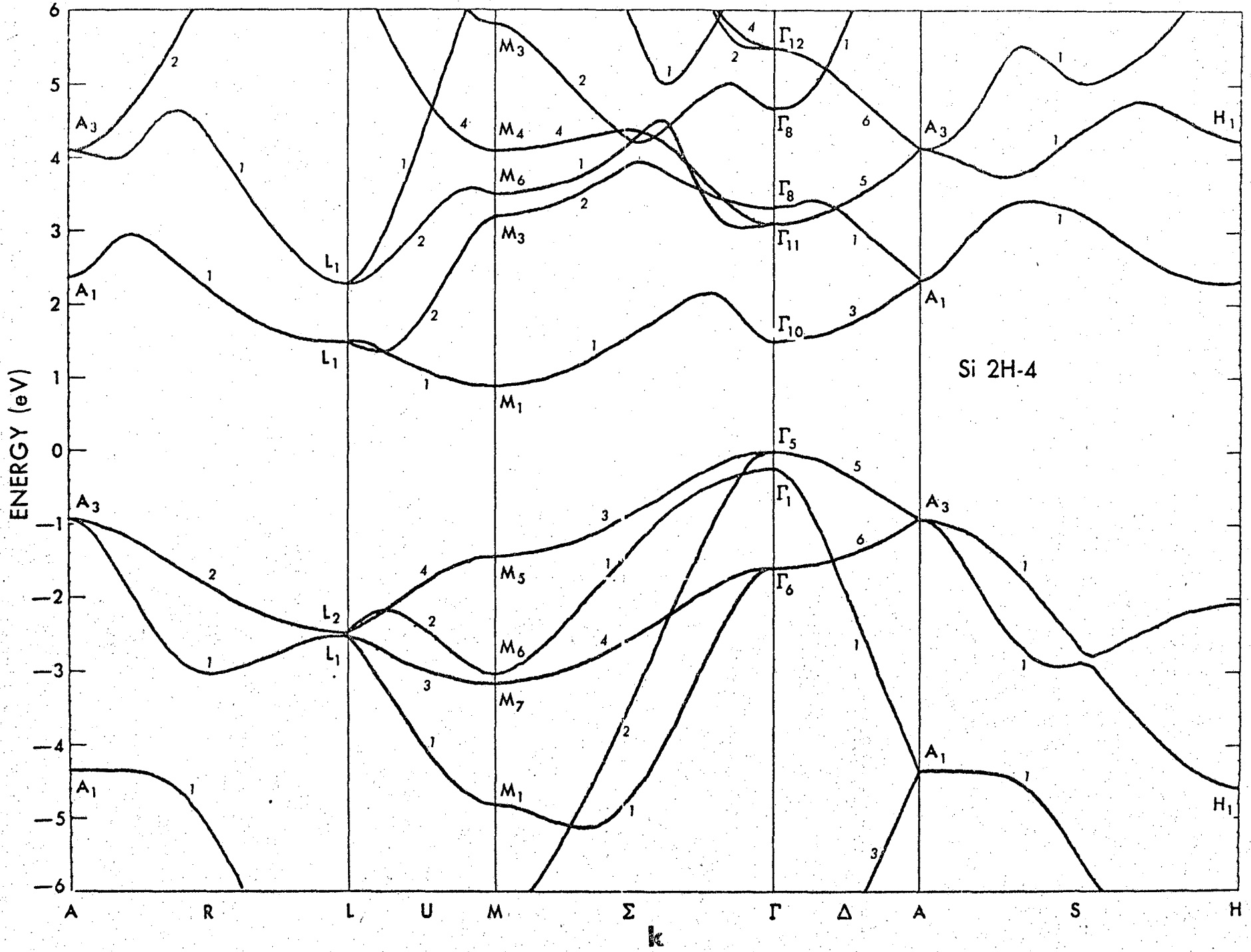
ENERGY (eV)
6
5
4
3
2
1
0
−1
−2
−3
−4
−5
−6
A
R
L
U
M
Σ
Γ
Δ
A
S
H
k
A3
A1
L1
L2
M3
M4
M6
M1
M5
M7
Γ12
Γ8
Γ11
Γ10
Γ5
Γ1
Γ6
H1
Si 2H-4

fig. 4.

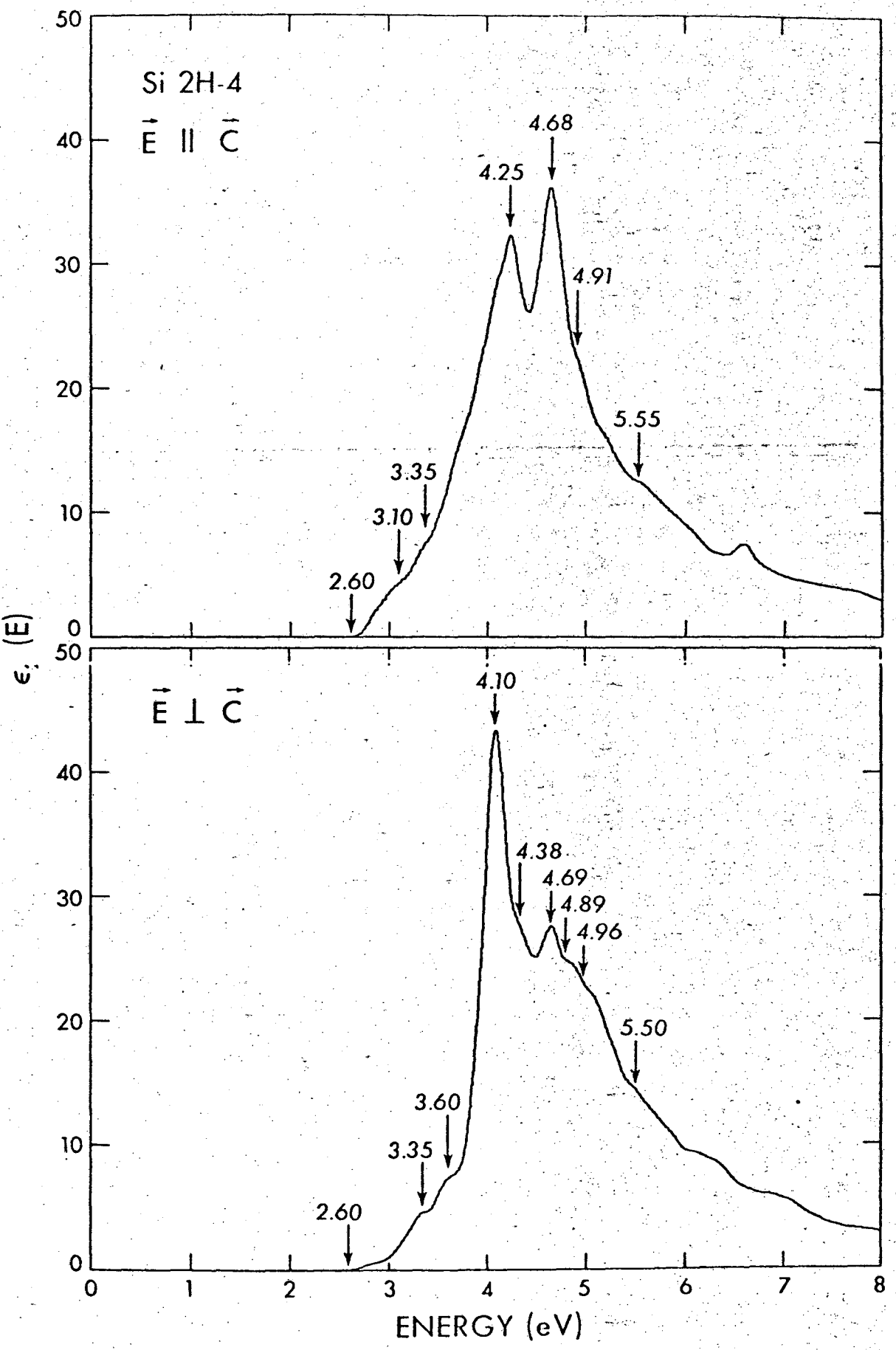
Si 2H-4
$\vec{E} \parallel \vec{C}$
4.68
4.25
4.91
5.55
3.35
3.10
2.60
$\vec{E} \perp \vec{C}$
4.10
4.38
4.69
4.89
4.96
5.50
3.60
3.35
2.60
ϵ_i (E)
ENERGY (eV)
0
10
20
30
40
50
0
1
2
3
4
5
6
7
8

Fig. 5

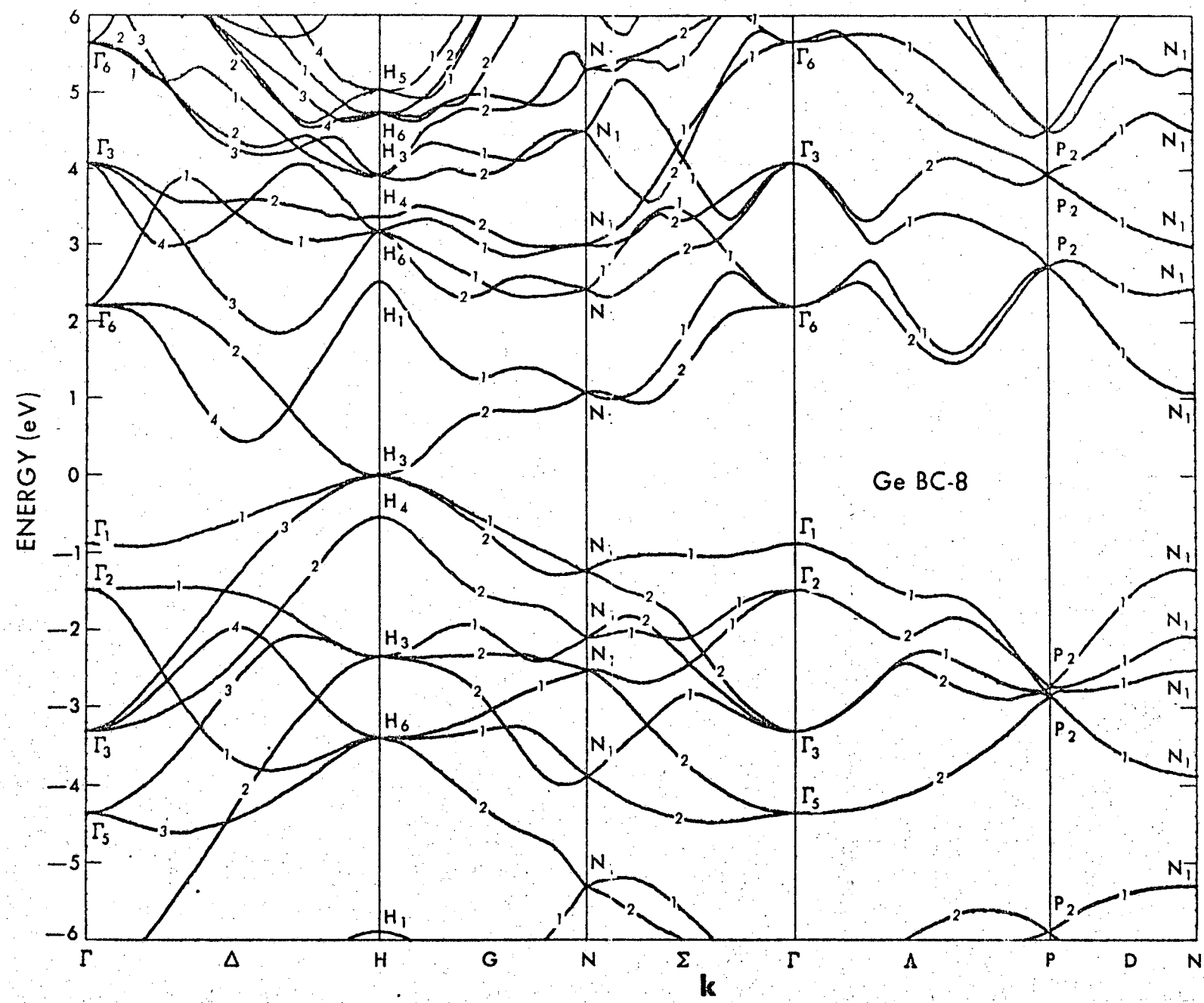

Fig. 6

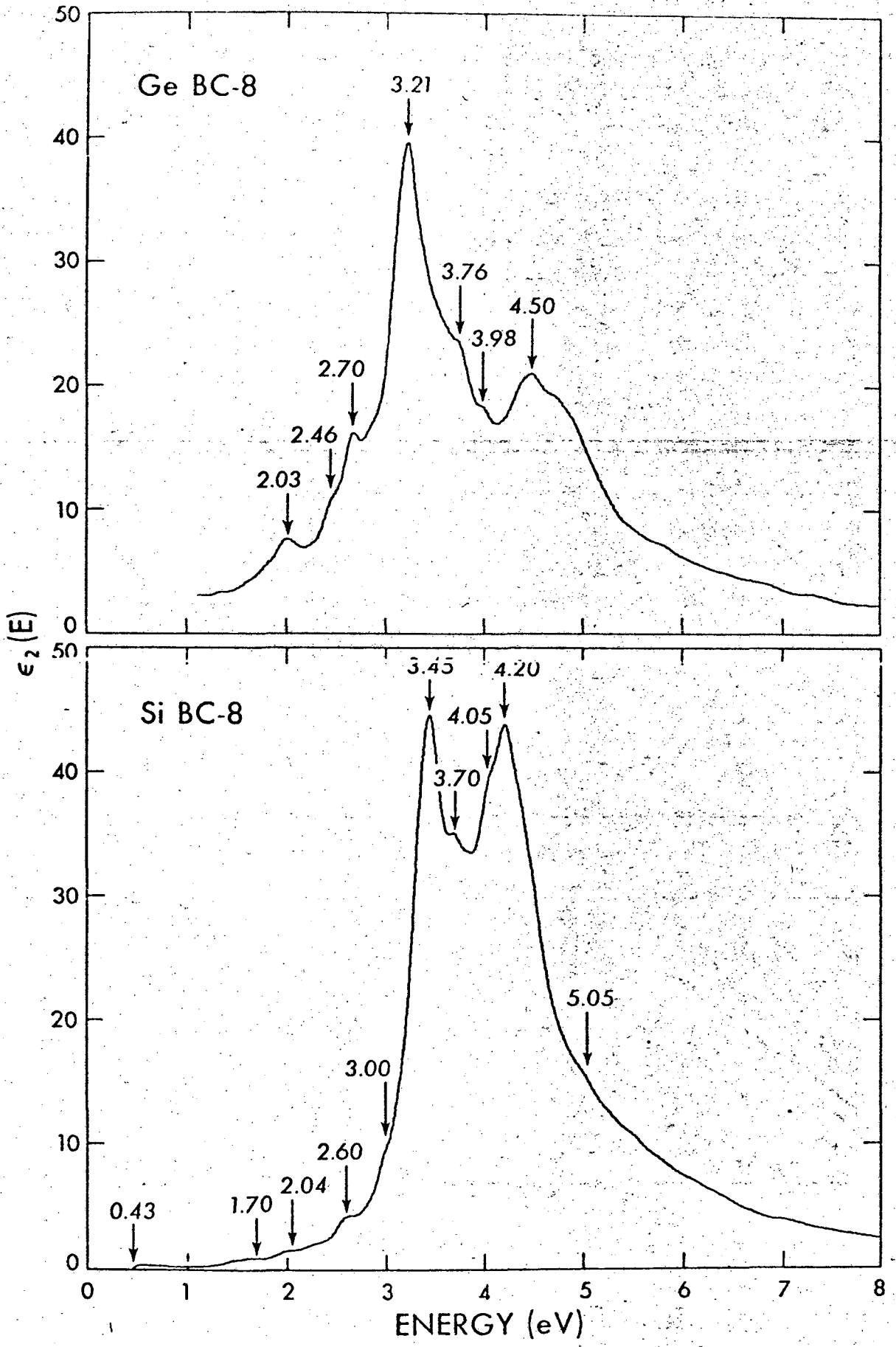
Ge BC-8
3.21
3.76
4.50
3.98
2.70
2.46
2.03
Si BC-8
3.45
4.20
4.05
3.70
5.05
3.00
2.60
2.04
1.70
0.43
$\epsilon_2(E)$
ENERGY (eV)

fig. 7

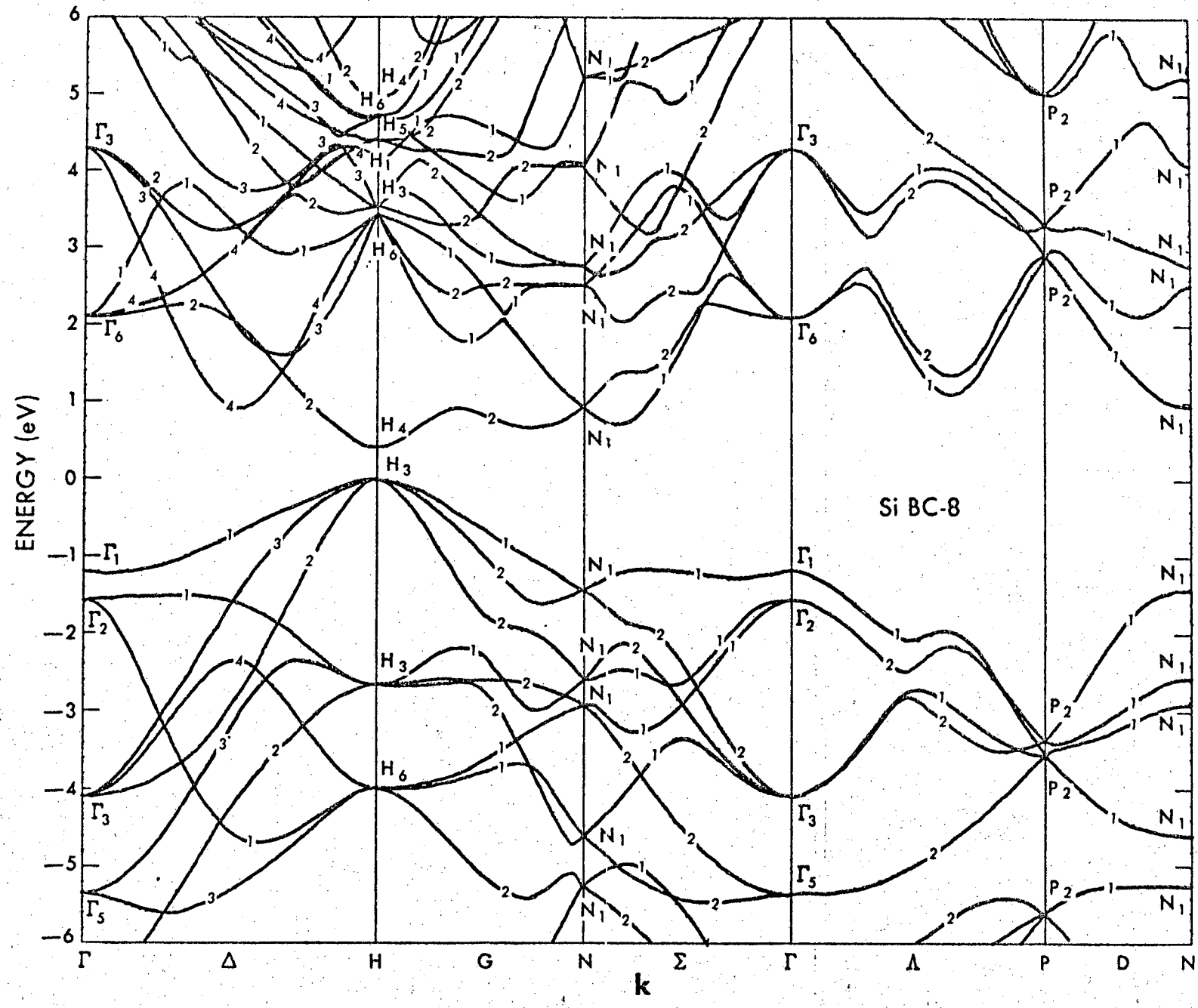
ENERGY (eV)
6
5
4
3
2
1
0
−1
−2
−3
−4
−5
−6
Γ
Δ
H
G
N
Σ
Γ
Λ
P
D
N
k
Si BC-8
Γ1
Γ2
Γ3
Γ5
Γ6
H1
H3
H4
H5
H6
N1
P2

Fig. 8

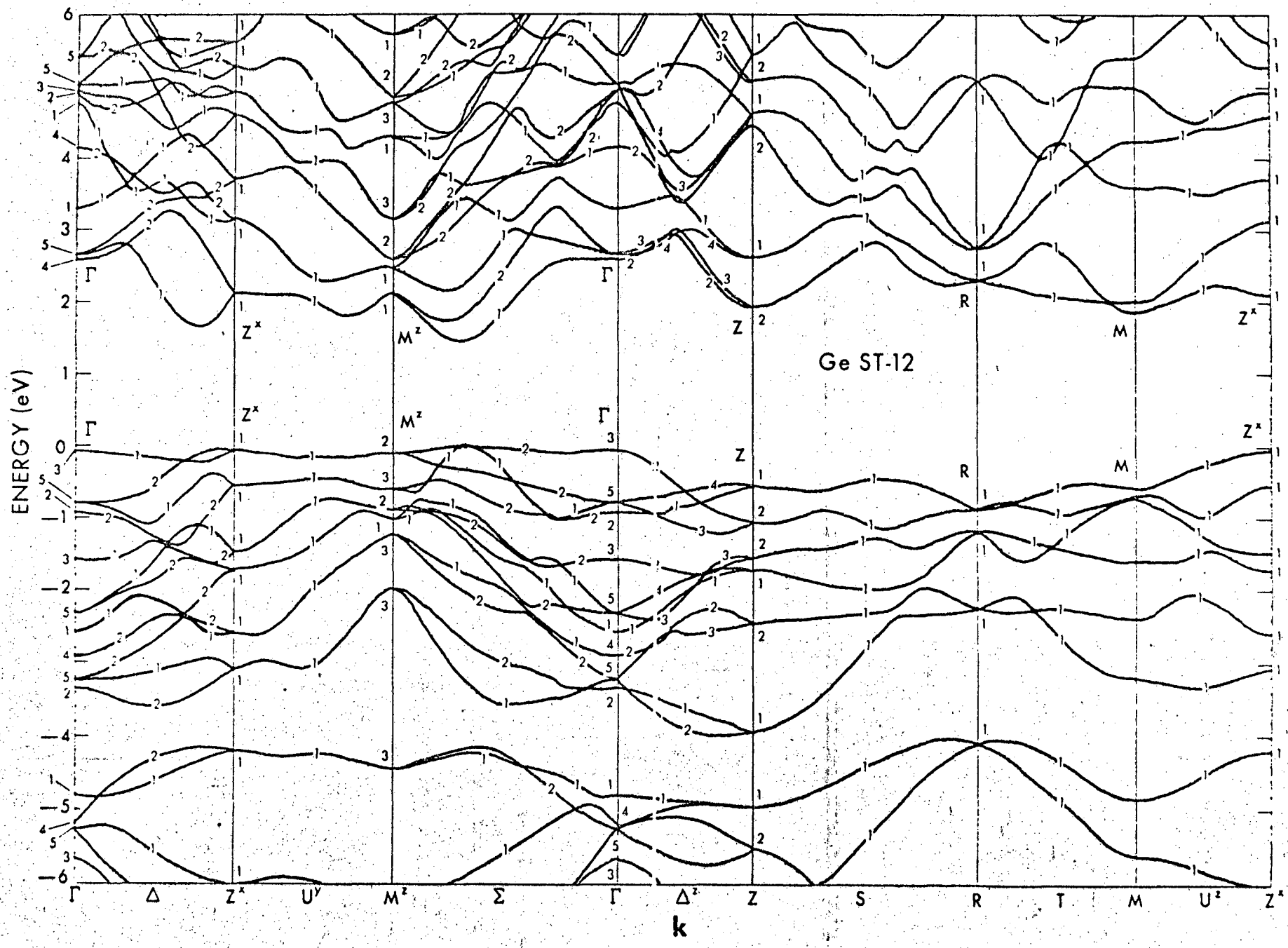

Fig 9

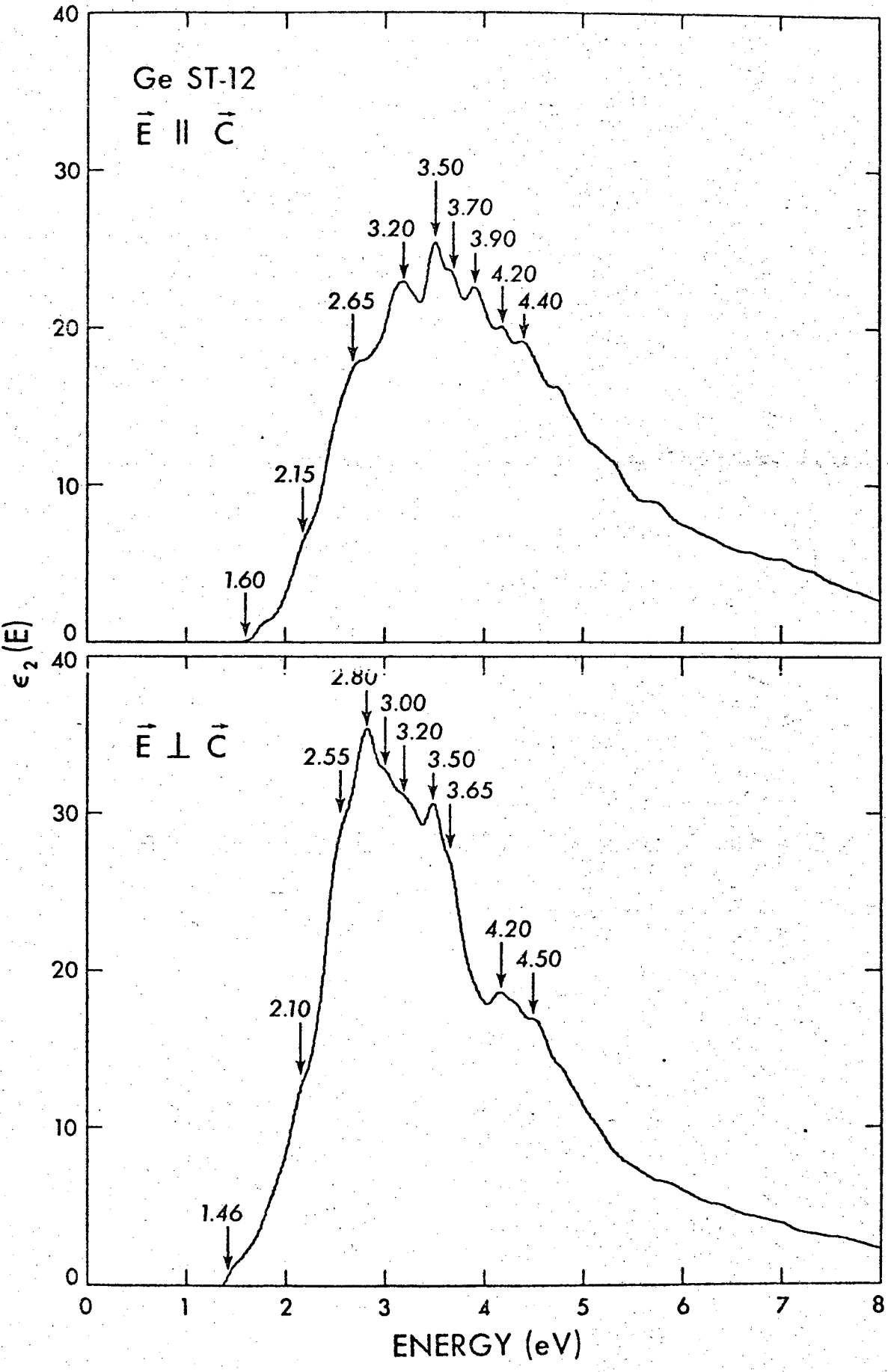

Fig. 10

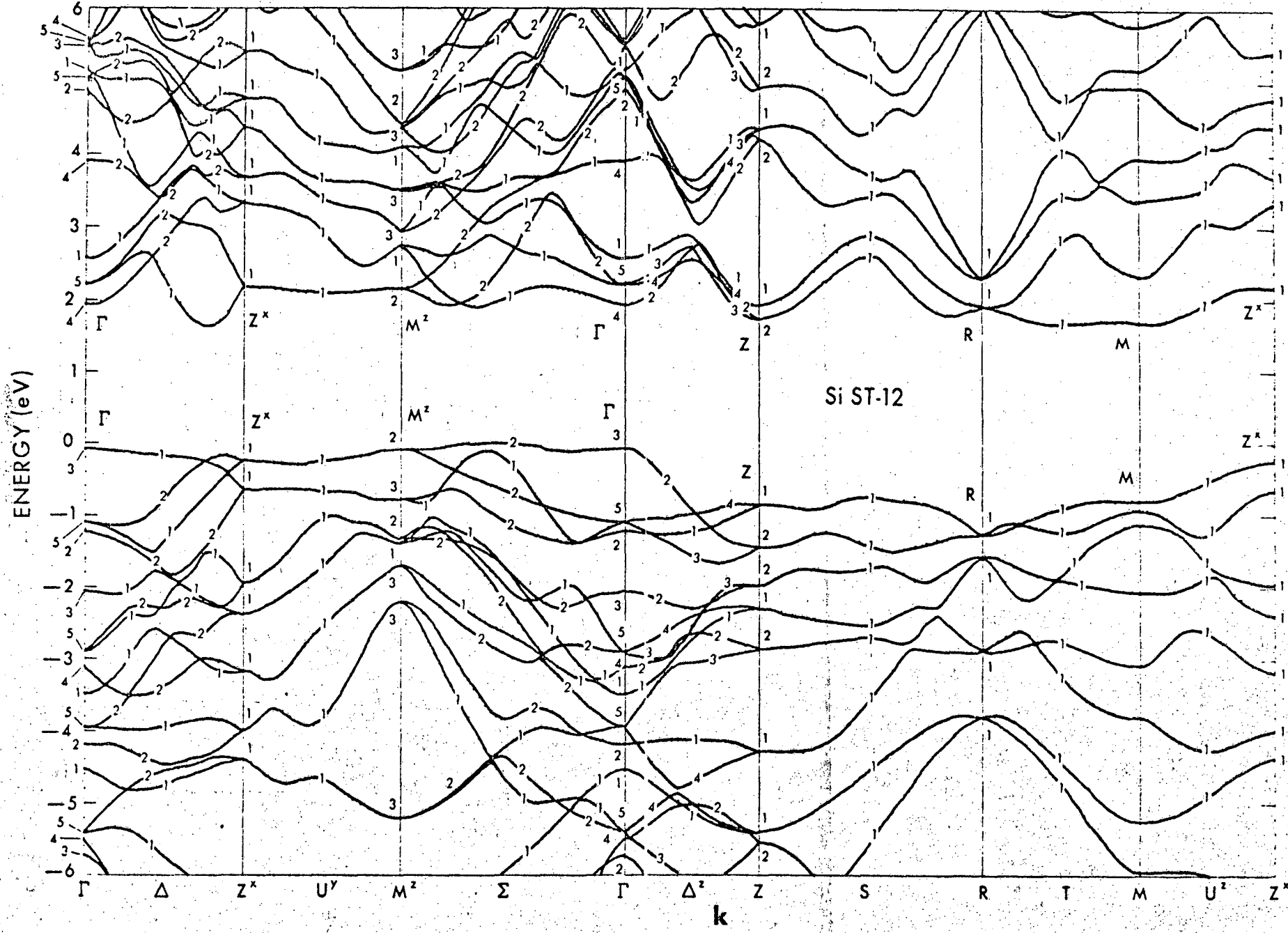

Fig. 11

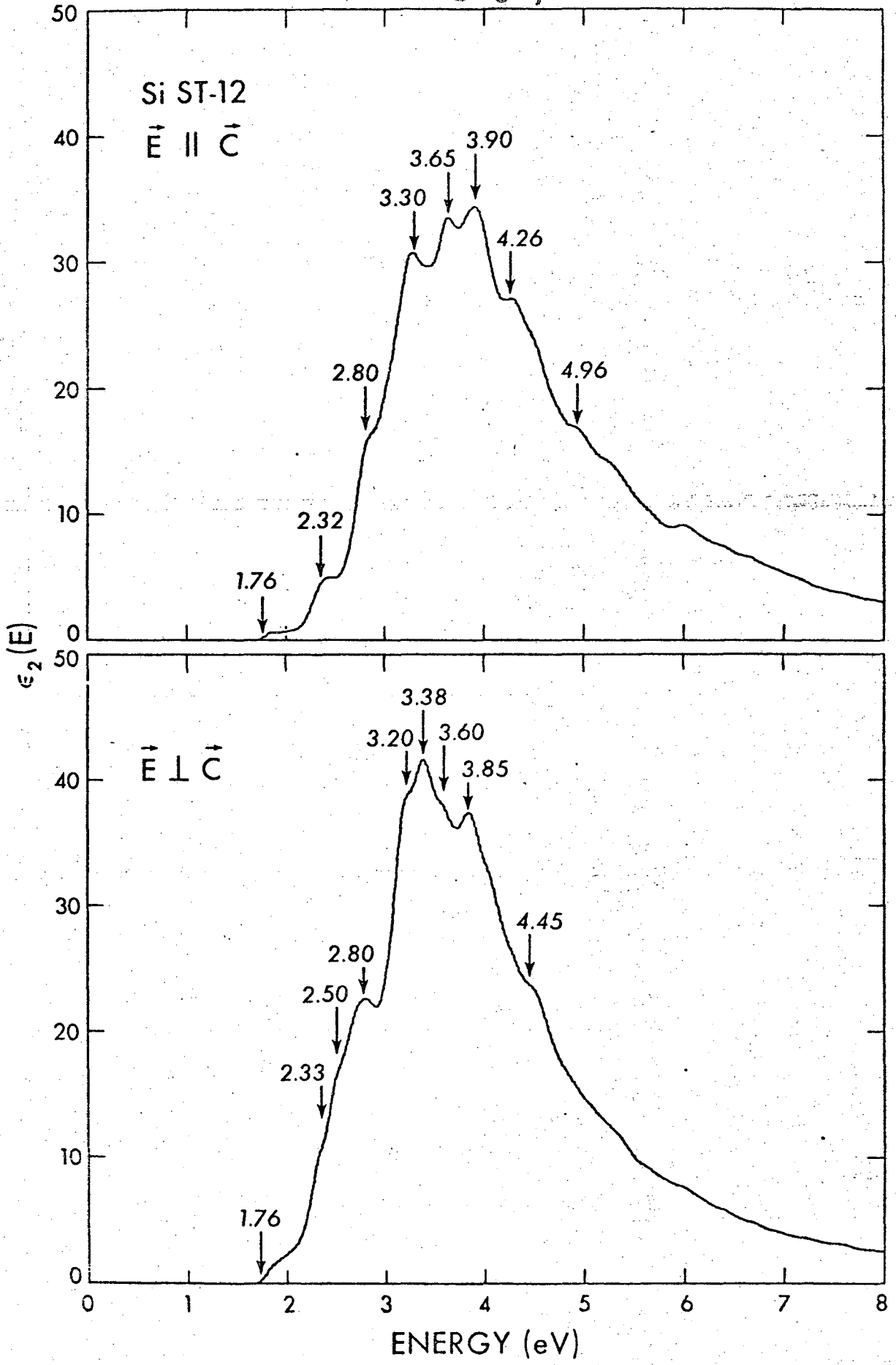

Fig. 12

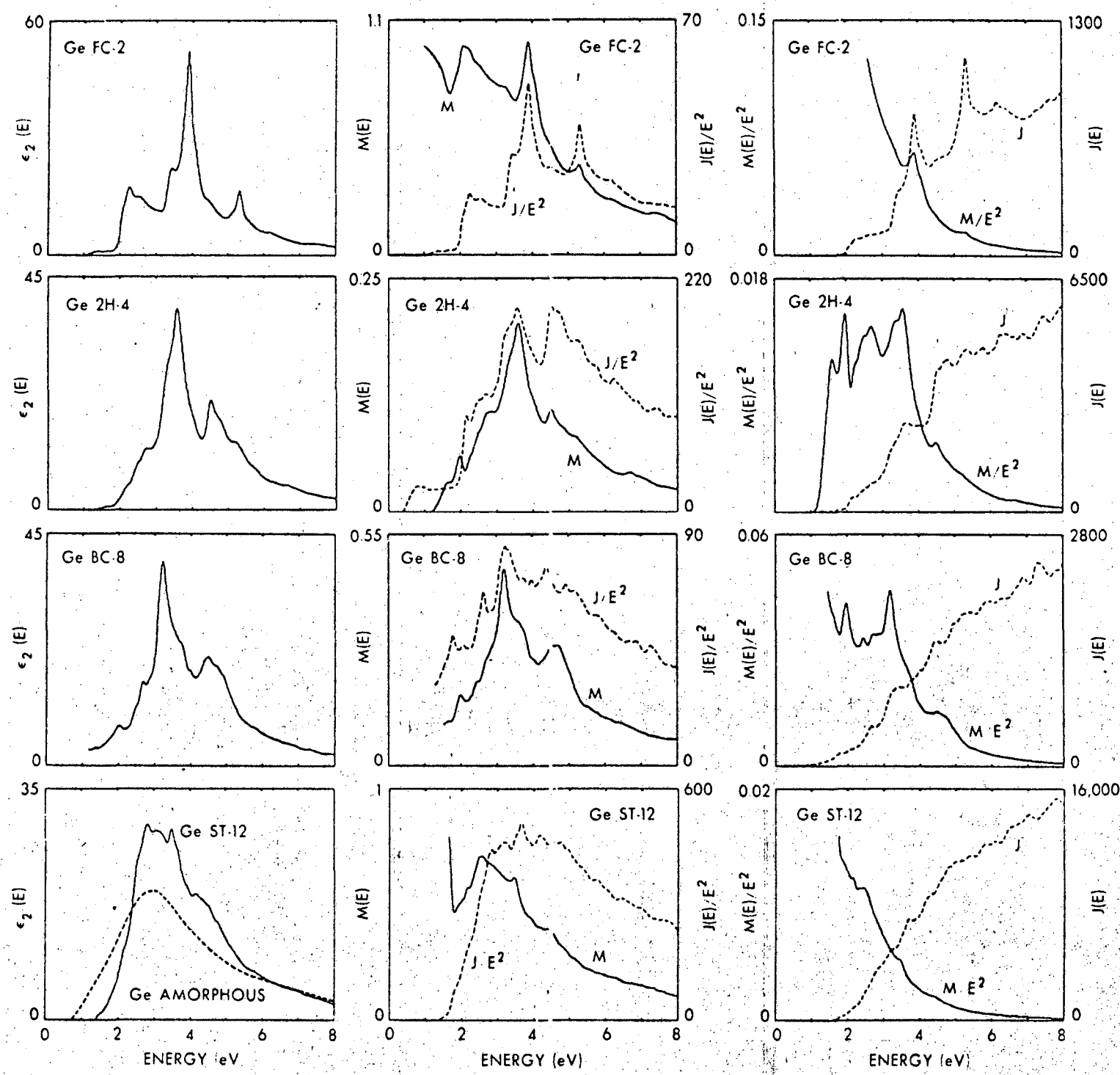
Ge FC-2
Ge 2H-4
Ge BC-8
Ge ST-12
Ge AMORPHOUS
ϵ_2 (E)
M(E)
J(E)/E²
M(E)/E²
J(E)
M
J/E²
J
M/E²
J E²
M E²
ENERGY (eV)
60
0
1.1
70
0.15
1300
45
0.25
220
0.018
6500
0.55
90
0.06
2800
35
1
600
0.02
16,000
0
2
4
6
8

Fig. 13

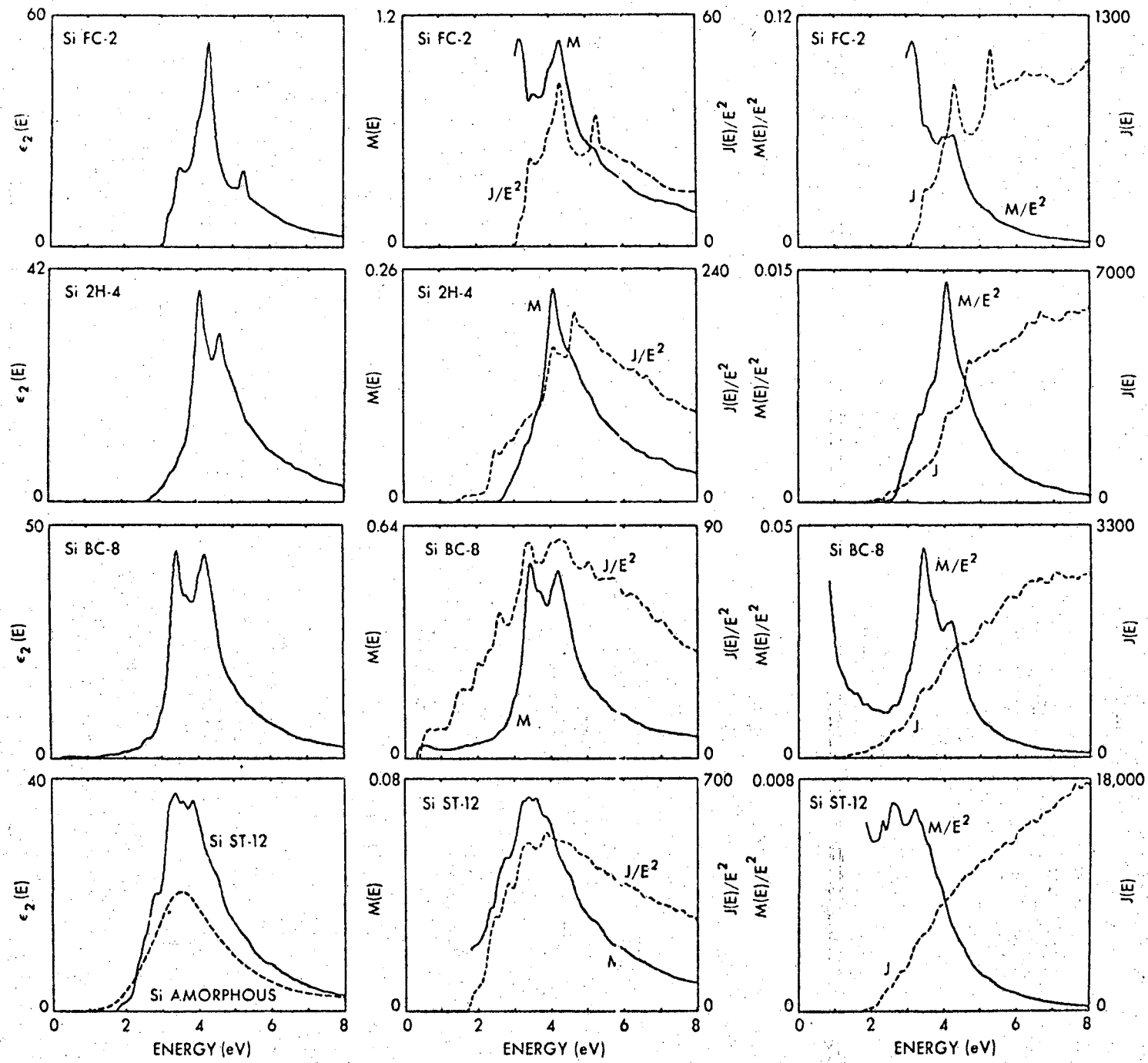
Si FC-2
Si 2H-4
Si BC-8
Si ST-12
Si AMORPHOUS
$\epsilon_2(E)$
M(E)
J(E)/E²
M(E)/E²
J(E)
M
J
J/E²
M/E²
ENERGY (eV)

Fig. 14

TECHNICAL INFORMATION DIVISION
LAWRENCE BERKELEY LABORATORY
UNIVERSITY OF CALIFORNIA
BERKELEY, CALIFORNIA 94720